

## SUBMILLIARCSECOND POLARIMETRIC IMAGING OF BLAZAR JETS AT 43 GHz

MATTHEW L. LISTER<sup>1</sup> AND ALAN P. MARSCHER

Department of Astronomy, Boston University, 725 Commonwealth Avenue, Boston, MA 02215

AND

W. K. GEAR

Mullard Space Science Laboratory, University College London, Holmbury St. Mary, Dorking, Surrey RH5 6NT, UK

Received 1997 December 18; accepted 1998 April 16

### ABSTRACT

We present 43 GHz polarization images obtained with the Very Long Baseline Array of four blazars (0829+046, 1055+018, 1334–127, and AP Librae), as well as four active galactic nuclei, which served as polarization calibrators (DA 193, OJ 287, 3C 279, and 1611+343). Six of these objects are members of the Nartallo et al. millimeter-wave polarization blazar monitoring sample. We find no differences in the overall millimeter-wave polarization properties of the BL Lacertae objects and quasars in our sample. This is in contrast to previous findings at centimeter wavelengths, in which the inferred magnetic fields of quasars are found to be predominantly aligned with the jet, while perpendicular configurations are found in BL Lac objects. With the exception of 1611+343, a low optical polarization quasar, all of the unresolved blazar cores in our sample have inferred magnetic field orientations perpendicular to the inner jet direction. Past nonimaging millimeter-wave polarization monitoring data have shown that these core orientations are stable in three of our sample objects; this may be due to strong, unresolved standing shocks located very close to the base of the jet. We also detect in the jets of blazars a moderate-sized population of polarized components having electric vectors that lie at an oblique angle to the local jet direction. We find that the observed distribution of electric vector misalignment angles cannot be fitted by a single population of oblique shocks having arbitrary inclinations with respect to the jet axis. Such a population predicts an overabundance of shocks with electric polarization vectors aligned with the jet axis, produced by relativistic effects associated with the jet flow. We find the data to be more consistent with a scenario in which the polarized jet components are merely enhanced regions whose magnetic field orientations are controlled by some mechanism other than shocks.

*Subject headings:* BL Lacertae objects: general — galaxies: active — galaxies: jets — polarization — quasars: general — shock waves

### 1. INTRODUCTION

Recent advances in polarization-sensitive very large baseline interferometry (VLBI) techniques at high frequencies have led to important new insights into the properties of blazars. This class of active galactic nuclei (AGNs), comprising BL Lacertae objects, and optically violent variable (OVV) quasars, displays highly energetic and rapid variability at all wavelengths, high fractional polarization, and core-dominated radio structure. At radio wavelengths, the bulk of the emission from blazars is synchrotron radiation from a relativistic jet that is assumed to be oriented very close to the line of sight. This scenario is responsible for the superluminal speeds of features seen moving down blazar jets in VLBI images, as well as the strong Doppler boosting of radiation in the observer frame. The superluminal features in VLBI jets have been modeled by various authors (e.g., Hughes, Aller, & Aller 1985; Marscher & Gear 1985) as transverse shocks in the jet flow, in which the initially tangled jet magnetic field is greatly compressed in one direction. These shocks appear in polarization-sensitive VLBI images as distinct regions with high fractional polarizations and electric vector position angles (EVPAs) parallel to the jet axis.

Although BL Lacs and OVV quasars share many common blazar characteristics, past VLBI polarization

studies (Cawthorne et al. 1993; Gabuzda et al. 1994) have revealed important differences at centimeter wavelengths. First, the EVPAs of quasar jets tend to be perpendicular to the jet axis, while in BL Lacs the electric vectors are aligned; second, the unresolved core components of quasars tend to have lower fractional polarizations than those of BL Lac objects. Cawthorne et al. (1993) have suggested that the jets of blazars start out with longitudinal and tangled  $B$  field components, but in quasars the longitudinal component gradually strengthens with distance from the core as a result of shear from the dense emission line gas near the nucleus. At large distances from the core, the shocks in quasars may be too weak to dominate the underlying field, resulting in an inferred magnetic field that is parallel to the jet. On the other hand, the downstream jet regions in BL Lacs may have smaller longitudinal/tangled  $B$  field ratios (Brown et al. 1994) and/or stronger transverse shocks (Gabuzda et al. 1994).

In the optical regime, the differences between BL Lacs and quasars are thought to originate in the broad-line region, located within  $\sim 1$  pc of the active nucleus. It is therefore logical to ask whether the above differences in jet polarization properties are still present in regions closer to the base of the jet. To address this question, millimeter- and submillimeter-wave observations are needed, since the lower opacities at these wavelengths allow us probe previously unresolved core regions on subparsec scales. Although continuum observations have revealed marked differences in the submillimeter spectral indices (Gear et al.

<sup>1</sup> Current address: Jet Propulsion Laboratory, California Institute of Technology, MS 238-332, 4800 Oak Grove Drive, Pasadena, CA 91109-8099.

TABLE 1  
SUMMARY OF IMAGE PARAMETERS

SOURCE	TYPE	RESTORING BEAM		TOTAL FLUX DENSITY (Jy)	rms (mJy beam <sup>-1</sup> )	PEAK/rms	FIGURE
		Size (mas)	P.A. (deg)				
0829+046 .....	IPOL	0.45 × 0.18	-4	0.942	0.9	747	1
	PPOL			0.076	0.7	59	...
1055+018 .....	IPOL	0.48 × 0.19	-7	3.418	1.4	1388	3
	PPOL			0.307	1.2	156	4
1334-127 .....	IPOL	0.58 × 0.20	-2	10.986	2.5	3719	5
	PPOL			0.573	2.8	164	...
AP Librae .....	IPOL	0.71 × 0.19	-8	1.600	1.9	433	6
	PPOL			0.053	1.4	14	...
DA 193 .....	IPOL	0.41 × 0.18	-17	2.736	1.5	1279	7
	PPOL			0.042	1.5	128	...
OJ 287 .....	IPOL	0.42 × 0.19	-7	1.700	1.3	1006	9
	PPOL			0.060	1.0	34	...
3C 279 .....	IPOL	0.50 × 0.20	-4	22.320	6.6	1995	10
	PPOL			1.045	5.2	116	...
1611+343 .....	IPOL	0.37 × 0.21	6	3.866	2.5	1170	12
	PPOL			0.167	3.1	26	...

1994) and flaring behavior (Stevens et al. 1994) of BL Lacs and quasars, polarization VLBI observations at frequencies > 22 GHz have shown the innermost jet components of several quasars to have BL Lac-like (aligned) EVPAs (Leppänen, Zensus, & Diamond 1995; Kembal, Diamond, & Pauliny-Toth 1996). Furthermore, Nartallo et al. (1998) have monitored the millimeter-wave EVPAs of a sample of blazars with the James Clerk Maxwell Telescope (JCMT), and find no differences in the polarization properties of the two classes. An important part of that study was to compare the continuum EVPAs to the position angle of the parsec-scale jet. High-resolution maps are needed for this purpose, since the jets of many AGNs are highly bent on subparsec scales (Krichbaum et al. 1994).

In this paper, we present submilliarcsecond-scale, polarization-sensitive 43 GHz VLBI observations of four objects in the Nartallo et al. (1998) blazar sample (0829+047, 1055+018, 1334-127, and AP Librae) for which high-resolution images were not available prior to our study. Our new images allow us to determine the position angle of the inner jet, which we compare to the core EVPA measured at 1.1 mm. In § 3 we discuss the inner magnetic field properties of these sources, along with four calibrators (DA 193, OJ 287, 3C 279, and 1611+343).

We discuss the general properties of our blazar sample in § 4. We find that a substantial number of VLBI components in blazars have EVPAs that lie at an oblique angle to the jet, which is not predicted by the simple transverse shock model. In § 5 we develop a model using oblique shocks based on the work of Cawthorne & Cobb (1990; hereafter CC90), and show that it also cannot adequately explain the observed EVPA misalignment distribution. In § 6 we discuss how the polarization properties of the VLBI components are more consistent with a simple nonshock model incorporating embedded, misaligned magnetic fields.

ten antennas of the Very Long Baseline Array (VLBA)<sup>2</sup> on 1996 November 23, from 9:00 to 21:00 UT. Observations of our program sources were interspersed with calibrators, which were carefully selected on the basis of known polarization structure, declination, compactness, and flux density, taking into account the special requirements of polarization-sensitive VLBI data processing (Leppänen et al. 1995). The data were recorded in eight baseband channels (IFs) using 1 bit sampling, each IF having a bandwidth of 8 MHz. Both right- and left-hand polarizations were recorded simultaneously in IF pairs, giving a total observing bandwidth of 32 MHz.

The data were correlated using the VLBA correlator in cross-polarization mode, with 2 s averaging. Each IF was subdivided into 16 spectral channels of 500 kHz bandwidth, and the right-, left-, and cross-circularly polarized visibilities (LL, RR, RL, and LR) were recorded on magnetic tape. Subsequent data analysis (i.e., editing and calibration) was performed at Boston University using the Astronomical Image Processing System (AIPS) software supplied by NRAO. The calibration procedure followed that of Leppänen et al. (1995).

Amplitude calibration was applied using the system temperatures measured at each antenna, along with gain curves supplied by the NRAO. The absolute flux density scale was established using concurrent flux-density measurements of OJ 287 taken at the Metsähovi Radio Observatory at 37 GHz. Prior to fringe fitting, the effects of parallactic angle rotation were removed from the right- and left-circular polarization (RCP and LCP) gains, so that these effects remained thereafter only in the polarization leakage factors for each antenna. These leakage factors (also called *D* factors) are complex numbers that characterize the polarization characteristics of the antenna feeds, and represent the amount of LCP signal being received by the RCP feed,

## 2. DATA ACQUISITION AND REDUCTION

The observations were carried out at 43 GHz using all

<sup>2</sup> The VLBA is a facility of the National Radio Astronomy Observatory, operated by Associated Universities Inc., under cooperative agreement with the National Science Foundation.

and vice versa.

Following a global fringe fit of the parallel-hand data, a cross-hand fringe fit was performed on a short scan of 3C 279, averaged over all baselines. The resulting RL phase and rate delay corrections were processed with the AIPS task POLSN and applied to the full data set using Los Alamos as a reference antenna.

A point-source model was used in conjunction with the task CALIB on each source to remove short-timescale atmospheric phase fluctuations and to increase coherence. The data were edited and then self-calibrated with a model of the source intensity distribution, using the standard iterative techniques of hybrid mapping described in the AIPS Cookbook (National Radio Astronomy Observatory 1990). The parameters of our images are given in Table 1.

In order to determine the  $D$  factor (feed) solutions for the antennas at the time of the observations, the task LPCAL (Leppänen 1995) was used on each source in our sample. Since these antenna-based factors are independent of source structure, we obtained a final set of  $D$  factors by taking an average of the solutions for all sources, omitting any values with deviations greater than  $3\sigma$  from the mean.

The instrumental EVPA correction for the data was established by examining the magnetic field orientation of polarized jet components in 3C 279 and 1055+018. The former source was observed several months earlier with the VLBA at 22 GHz by Ojha (1997) and at 15 GHz by Homan et al. (1998). It was found to contain a polarized component (C4) with an electric field exactly parallel to the component's position angle measured with respect to the core, which was located  $\sim 3.2$  mas to the northeast. The quasar 1058+018 also contained a strong component  $\sim 2$  mas to the northwest of the core, with EVPA parallel to the jet, as verified with the VLBA at 5 GHz in 1996 January by Attridge, Roberts, & Wardle (1998).

### 3. ANALYSIS OF INDIVIDUAL SOURCES

In this section we present the results of our 43 GHz polarization-sensitive VLBI observations. We performed Gaussian model fits to the sources in the  $u$ - $v$  plane using the task MODELFIT in the CalTech VLBI package (Shepherd, Pearson, & Taylor 1994). The results of these fits are given in Table 2, and are intended as a general guideline for the source descriptions that follow. We caution that this type of model fitting does not always produce unique results, especially for regions of nearly continuous jet emission. While an accurate parametrization of errors is extremely difficult with this method, we estimate the given positions of strong, isolated components to be accurate to within a quarter of a beamwidth (see Table 1). The fits are less reliable for very weak components and those located in regions of diffuse emission.

The last three columns of Table 2 give the Stokes  $I$  flux density, EVPA, and ratio of  $P$  to  $I$  flux at the central peak of the Gaussian component. The latter quantity can be identified with the fractional polarization  $m$  (albeit with no correction made for Ricean bias; see Wardle & Kronberg 1974), and is an indicator of the degree of order in the magnetic field. We caution that in some cases the peak of polarized emission is offset from that of the total emission, so that the values given in Table 2 may not represent the maximum fractional polarization associated with a particular  $I$  component.

No rotation measurement corrections were applied to the

observed EVPAs, because rotation measures for these and other AGNs at arcsecond scales (e.g., Carvalho 1985; Broten, MacLeod, & Vallee 1988) imply very small Faraday rotations ( $\lesssim 5^\circ$ ) at 43 GHz. The inferred magnetic field vectors are therefore assumed to be perpendicular to the electric vectors in our images. Throughout this paper we use a cosmological constant  $q_0 = 0$  and a Hubble constant  $h = 0.65$ , where the units of  $h$  are  $100 \text{ km s}^{-1} \text{ Mpc}^{-1}$ . We define the spectral index such that the flux density  $S_\nu$  is proportional to  $\nu^\alpha$ .

### 3.1. Program Sources

#### 3.1.1. 0829+046

This flat-spectrum BL Lacertae object ( $z = 0.18$ ) is very active in the optical and IR regimes, showing large changes in polarization and total intensity on daily timescales (Holmes et al. 1984; Pica et al. 1988; Smith et al. 1987; Wills et al. 1980). Its high optical polarization (ranging up to 28%; Sitko, Schmidt, & Stein 1985) and variability are typical of the blazar class. This source has been detected in both X-rays (Brinkmann et al. 1995) and gamma rays (McLaughlin et al. 1996; Fichtel et al. 1994).

On arcsecond scales, 0829+046 has a very strong core and a highly curved jet extending to  $\sim 30''$  (Antonucci & Ulvestad 1985). The jet has a P.A. =  $130^\circ$  close to the core, and bends sharply to P.A. =  $235^\circ$  at  $r \simeq 13''$  ( $26 h^{-1}$  kpc). The only previously published VLBI maps of this source are a 15 GHz image by Kellermann et al. (1998) and several 22 GHz VLBA observations at epochs 1996.6, 1996.9, and 1997.58 by Marscher et al. (1998).

In our 43 GHz image (Figs. 1 and 2), this source displays a well-defined jet extending to the northeast, starting at P.A.  $\simeq 62^\circ$  and bending to P.A.  $\simeq 81^\circ$  at  $r \simeq 1$  mas. A comparison with the epoch 1996.6 map of Marscher et al. (1998) shows very little change in morphology in the inner 2 mas, where the contours are the most reliable. The derived upper limit on the proper motion of component C1 is  $0.26 \text{ mas yr}^{-1}$ , which implies that  $\beta_{\text{app}} \lesssim 2.0 h^{-1}$ . Typical Doppler factors used in emission models for other gamma-ray-loud blazars range from  $\delta = 11$  for Mk 501 (Comastri et al. 1997) and  $\delta = 13$  for 0528+134 (Sambruna et al. 1997) to  $\delta = 19$  for 0836+710 (Comastri et al. 1997). Given the upper limit on  $\beta_{\text{app}}$  for 0829+046, a small viewing angle is needed to obtain a reasonably high  $\delta$  (e.g., for  $\delta > 5$  and  $h = 0.65$ ,  $\theta \lesssim 10^\circ$ ). The large apparent misalignment of the parsec- and kiloparsec-scale jets may be the result of jet curvature exaggerated by a small viewing angle.

The polarization structure of this source consists of emission from regions near the core (D) and C1–C2. The approximate fractional polarization in these regions is  $\sim 6\%$  and  $\sim 17\%$ , respectively. Although the high fractional polarization near C1–C2 is consistent with the idea that BL Lacs have strong shocks (e.g., Cawthorne et al. 1993), the EVPA in this region does not indicate a perpendicularly compressed magnetic field as expected. It instead appears to lie at an oblique angle to the local jet direction. Possible reasons for this will be discussed in § 4.3.

The EVPA of the core region ( $45^\circ$ – $46^\circ$ ) is fairly well aligned with the jet direction defined by components C1, C2, and C3. Nartallo et al. (1998) measured the millimeter-wave EVPA at two epochs (1992.81 and 1993.15), and found it to decrease from  $46^\circ$  to  $40^\circ$  as the fractional polarization decreased. The University of Michigan monitoring data show that the integrated EVPA of the entire source at 8

TABLE 2  
VLBI COMPONENT PROPERTIES

COMPONENT	GAUSSIAN FIT PARAMETERS <sup>a</sup>						VALUES AT CENTRAL PEAK		
	<i>r</i> (mas)	P.A. (deg)	Total <i>I</i> (Jy)	<i>a</i> (mas)	<i>a/b</i>	$\phi$ (deg)	<i>I</i> (Jy beam <sup>-1</sup> )	EVPA (deg)	<i>m</i> <sup>b</sup>
0829+046									
D .....	...	...	0.591	0 <sup>c</sup>	...	...	0.311	45	0.06
C4 .....	0.11	89	0.101	0	...	...	0.156	46	0.09
C3 .....	0.35	52	0.024	0	...	...	0.014	...	...
C2 .....	0.56	59	0.029	0	...	...	0.021	18	0.20
C1 .....	0.68	63	0.065	0	...	...	0.034	19	0.17
1055+081									
D .....	...	...	1.566	0	...	...	0.852	-55	0.09
C2 .....	0.23	-63	1.377	0.14	0.60	-70	0.609	-73	0.07
C1 .....	1.95	-46	0.116	0.33	0.45	-45	0.031	-44	0.12
1334-127									
D .....	...	...	8.381	0.07	0.36	-37	4.213	153	0.05
C3 .....	0.28	139	1.400	0.30	0.28	-44	0.881	102	0.07
C2 .....	0.94	142	0.038	0	...	...	0.018	...	...
C1 .....	2.65	153	0.027	0	...	...	0.010	...	...
AP Librae (1514-241)									
D .....	...	...	0.649	0	...	...	0.361	...	...
C2 .....	0.46	171	0.219	0	...	...	0.240	...	...
C1 .....	0.93	172	0.203	0	...	...	0.121	117	0.07
DA 193 (0552+398)									
D .....	...	...	0.370	0.29	0.83	-31	0.156	-76	0.03
C5 .....	0.18	-98	1.596	0.07	0.77	-14	0.831	-138	0.01
C4 .....	0.32	-87	0.300	0.13	0.58	-15	0.342	-167	0.02
C3 .....	0.39	-117	0.157	0.41	0.34	-51	0.111	...	...
C2 .....	0.74	-81	0.086	0.77	0.46	51	0.008	...	...
C1 .....	2.22	-51	0.010	0	...	...	0.006	...	...
OJ 287									
D .....	...	...	0.972	0	...	...	0.559	-119	0.02
C6 .....	0.12	-93	0.396	0.23	0.07	47	0.292	-108	0.04
C5 .....	0.61	-95	0.018	0	...	...	0.009	-45	0.36
C4 .....	0.79	-92	0.017	0	...	...	0.012	...	...
C3 .....	1.03	-95	0.079	0.44	0.64	0	0.016	...	...
C2 .....	1.30	-91	0.020	0	...	...	0.012	...	...
C1 .....	1.50	-91	0.012	0	...	...	0.006	...	...
3C 279									
D .....	...	...	7.499	0	...	...	5.710	-115	0.01
C8 .....	0.16	-132	10.718	0.27	0.30	63	4.344	-118	0.06
C5 .....	1.19	-128	0.102	0	...	...	0.042	...	...
C4 .....	3.18	-115	1.587	0.44	0.39	-25	0.423	-115	0.15
1611+343									
D .....	...	...	1.921	0	...	...	1.298	94	0.02
C7 .....	0.09	167	0.988	0.24	0.34	-9	1.176	90	0.03
C6 .....	0.43	157	0.087	0.26	0.40	63	0.057	125	0.22
C5a .....	1.38	172	0.054	0.66	0.23	-23	0.007	...	...
C3 .....	2.21	180	0.078	0.37	0.59	-13	0.018	136 <sup>d</sup>	0.60 <sup>d</sup>

<sup>a</sup> *a* = major axis, *a/b* = axial ratio,  $\phi$  = position angle of major axis.

<sup>b</sup>  $m = (Q^2 + U^2)^{1/2}/I$ , where *I*, *Q*, and *U* are Stokes parameters.

<sup>c</sup> Indicates  $\delta$ -function component.

<sup>d</sup> Measured at *P* peak position. Value uncertain due to low *P* flux density.

GHz is aligned with the parsec-scale jet P.A. during 1996, at which time *m* was increasing. These data are consistent with a steady, transverse magnetic field in the core of this source.

3.1.2. 1055+018

The high optical polarization quasar (HPQ) 1055+018

(*z* = 0.888) was first classified as a blazar by Impey & Tapia (1990). Its overall spectrum in the radio region is relatively flat, with a turnover at ~15 GHz (Gear et al. 1994). This source has also been the subject of extensive multifrequency monitoring in the radio-to-millimeter regime. The light curves show flares that typically occur every 1–2 yr and

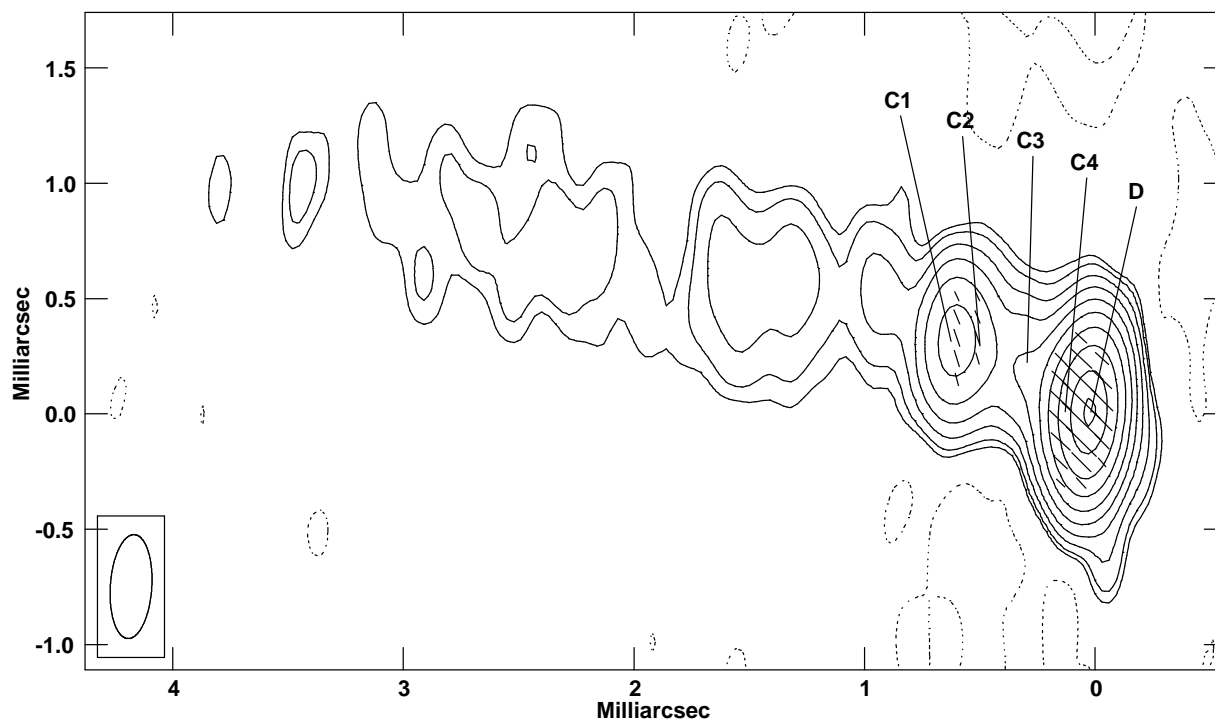


FIG. 1.—VLBA total intensity (Stokes I) image of 0829+047 at 43 GHz, epoch 1996.90, with electric polarization vectors superimposed. Contours are  $-0.3\%$ ,  $0.3\%$ ,  $0.5\%$ ,  $1\%$ ,  $2\%$ ,  $4\%$ ,  $8\%$ ,  $16\%$ ,  $32\%$ ,  $64\%$ , and  $95\%$  of the peak brightness,  $697 \text{ mJy beam}^{-1}$ . The polarization vectors are scaled such that  $1 \text{ mas} = 185 \text{ mJy beam}^{-1}$ .

slowly decay over a  $\sim 0.9 \text{ yr}$  timescale (Teräsraanta & Valtaoja 1994).

On arcsecond scales, this quasar displays a classical triple structure  $30''$  in extent, with a well-defined kiloparsec-scale jet at a P.A. of  $180^\circ$  (Murphy, Browne, & Perley 1993). It has also been studied at several epochs using low-frequency ( $< 1.7 \text{ GHz}$ ) VLBI (Romney et al. 1984; Padrielli et al. 1986, 1991; Altschuler et al. 1995; Bondi et al. 1996). These maps

show a jet  $\sim 25 \text{ mas}$  in length at P.A.  $\sim -63^\circ$ . At higher frequencies, few VLBI maps are available for this source. A  $15 \text{ GHz}$  map of Kellermann et al. (1998) shows a twisting jet  $10 \text{ mas}$  in length, starting at P.A.  $= -47^\circ$  and curving toward P.A.  $= -77^\circ$  at  $r \simeq 3 \text{ mas}$ . A polarization image made at  $5 \text{ GHz}$  by Attridge et al. (1998) shows a jet electric field orientation that is aligned parallel to the local jet direction ( $-47^\circ$ ).

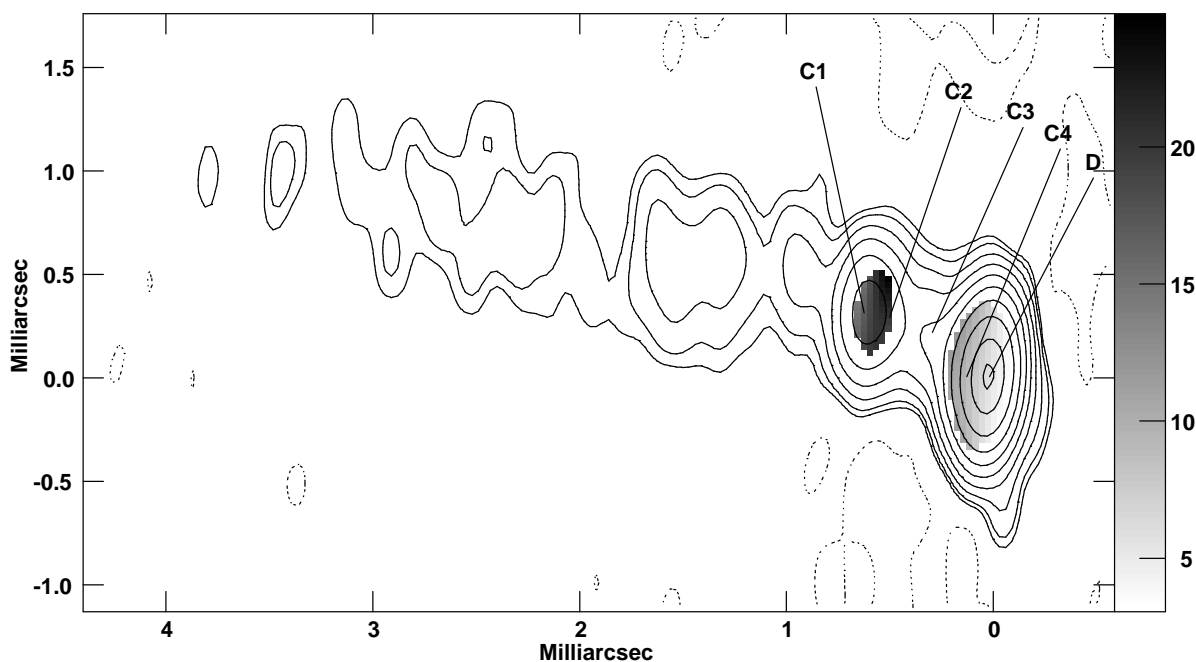


FIG. 2.—VLBA total intensity (Stokes I) image of 0829+047 at 43 GHz, epoch 1996.90, with contours as in Fig. 1. The linear gray scale corresponds to the fractional polarization ( $P/I$ ) in percent.

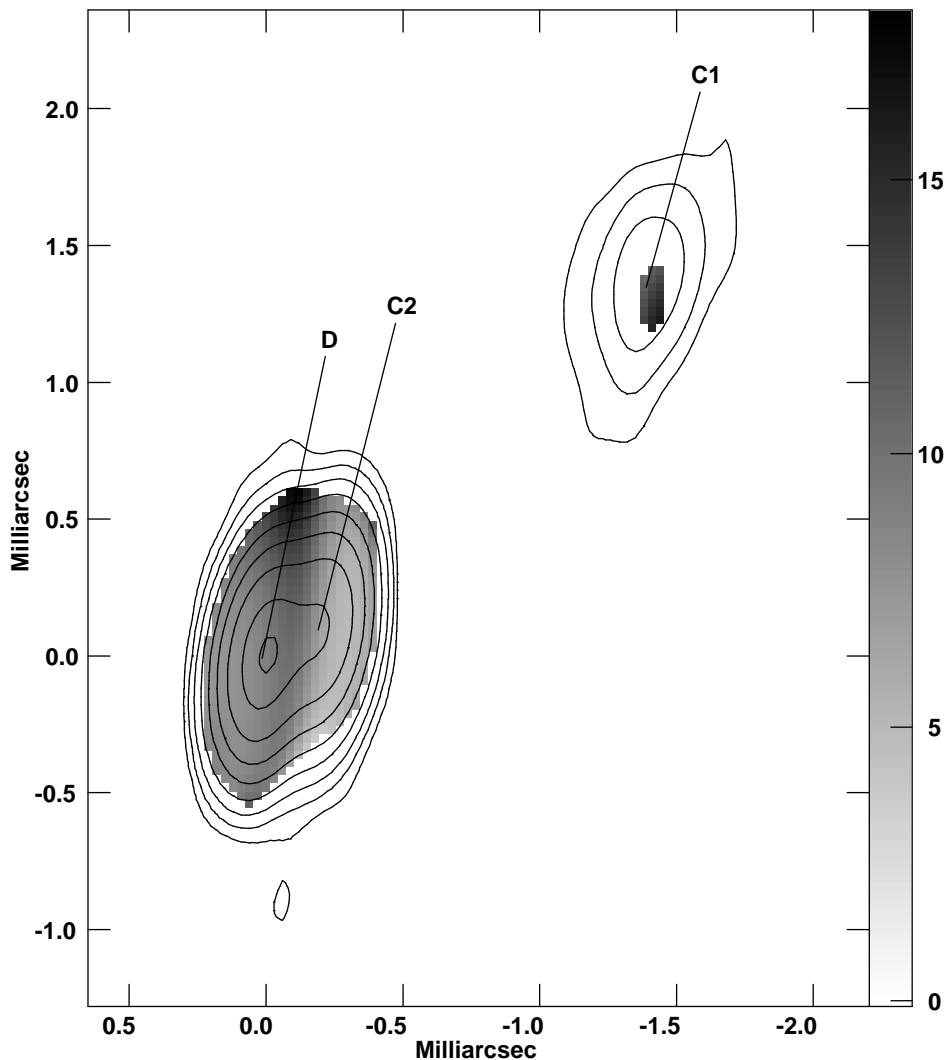


FIG. 3.—VLBA total intensity image of 1055+018 at 43 GHz, epoch 1996.90. Contours are  $-0.45\%$ ,  $0.45\%$ ,  $1\%$ ,  $2\%$ ,  $4\%$ ,  $8\%$ ,  $16\%$ ,  $32\%$ ,  $64\%$ , and  $95\%$  of the peak brightness,  $1.927 \text{ Jy beam}^{-1}$ . The linear gray scale corresponds to the fractional polarization in percent.

A total intensity contour image of 1055+018 at 43 GHz is presented in Figure 3. This image can be model-fitted by three components, listed in Table 2. Extending outward from the core (D), there is a component (C2) at  $r = 0.23$  mas, and a more extended component (C1) at  $r = 1.95$  mas. The latter component also appears in two 15 GHz images (epochs 1996.82 and 1995.57) of Kellermann et al. (1998), with a proper motion of  $0.19 \pm 0.05 \text{ mas yr}^{-1}$ , corresponding to an apparent speed of  $\sim 6h^{-1}c$ .

No positional information is available for component C2 at other epochs. However, the University of Michigan radio data indicate a sudden increase in polarized flux density at 5 and 14.5 GHz, as well as a change in the total EVPA at 5 GHz, beginning in  $1995.7 \pm 0.1$ . Such flares are accompanied in many sources by the emergence of a new jet component, as in the case of BL Lac (Mutel et al. 1990). If the 1995.7 flare is associated with the birth of the polarized component C2, its position at  $r = 0.23$  mas in Figure 4 gives a proper motion of  $0.19 \pm 0.02 \text{ mas yr}^{-1}$ , which is consistent with the speed of C1 as estimated above.

The polarized emission at 43 GHz from 1055+018 is shown in Figure 4. All three components are present in the polarized image, with D, C2, and C1 having approximate fractional polarizations of 9%, 7%, and 12%, respectively

(Table 2). The peak of the polarized emission associated with C1 is slightly offset from the  $I$  peak (Fig. 3).

The EVPA of this source starts out at the core aligned approximately with the direction of C1. It then gradually rotates toward the direction of C2, where it appears to become misaligned with respect to the jet. The latter component has a different P.A. C1, which may indicate a slight bend in the jet at this location. Higher resolution observations are required to determine whether the EVPA is aligned with the jet near C2, as it is near components D and C1.

The transverse  $B$ -field orientation in the core of this source is not that expected of a quasar, based on previous centimeter-wave results (Cawthorne et al. 1993; Gabuzda et al. 1994). The University of Michigan monitoring data indicate a large flare beginning in 1996.6, and if a VLBI component with a strongly perpendicular  $B$  field were ejected at that time, it would dominate the integrated EVPA of the source. The integrated EVPA has remained fairly steady over the past 5 yr, however, to within  $\sim 40^\circ$ . At 14.5 GHz, the monitoring data show a mean EVPA of  $\sim -50^\circ$ , with a value of  $-58^\circ$  at the epoch of our 43 GHz image. Nartallo et al. (1998) find similar EVPAs of  $-63^\circ$  (epoch 1993.15) and  $-58^\circ$  (epoch 1995.9) at 273 GHz. These data suggest

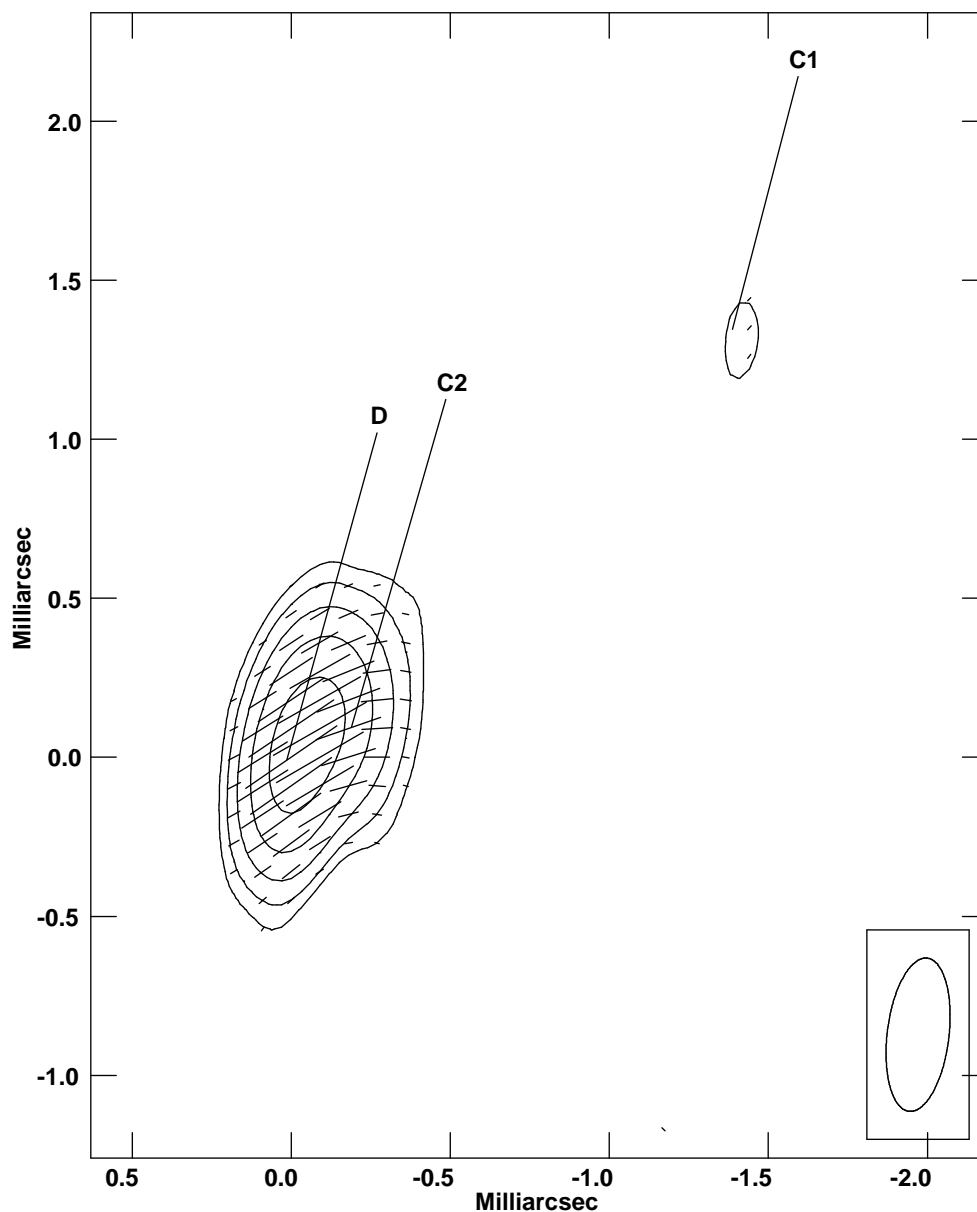


FIG. 4.—Linearly polarized intensity ( $P$ ) image of 1055+018, with electric vectors superimposed. Contours are  $-4\%$ ,  $4\%$ ,  $8\%$ ,  $16\%$ ,  $32\%$ , and  $64\%$  of the peak brightness,  $180 \text{ mJy beam}^{-1}$ . The polarization vectors are scaled such that  $1 \text{ mas} = 619 \text{ mJy beam}^{-1}$ .

either that the underlying magnetic field is perpendicular, or that this source has one or more stationary components near the core with transverse magnetic field orientations that dominate the observed polarization properties.

### 3.1.3. 1334–127

The high optical polarization blazar 1334–127 ( $z = 0.539$ ) was originally included in the Kühn & Schmidt (1990) BL Lac catalog, but was subsequently reclassified as a quasar by Stickel, Kühn, & Fried (1993). Its radio spectrum is quite flat in the radio-to-millimeter range (0.3–100 GHz) (Impey & Neugebauer 1988). On arcsecond scales, the radio structure consists of a core and a continuous jet that curves east of the core out to  $6''.5$  (Perley 1982). Past VLBI observations (Fey, Clegg, & Fomalont 1996) indicate a very straight jet extending to  $\sim 30 \text{ mas}$  along P.A. =  $148^\circ$ .

The total intensity image of 1334–127 at 43 GHz is presented in Figure 5. There is a continuous jet along

P.A.  $\sim 140^\circ$  out to  $\sim 1.5 \text{ mas}$  from the core. The jet then becomes less defined, with an area of weak, diffuse emission to the southeast of the core. A slightly extended component (C1) is located at  $r = 2.6 \text{ mas}$ , P.A. =  $152^\circ$  (see Table 2).

The polarized emission is located near the core (D) and component C3, with approximate fractional polarization values of  $5\%$  and  $7\%$  at the  $I$  peak positions. The EVPA of the core is oriented at  $153^\circ$ , which aligns well with the location of component C1, but not with C2 or C3. The EVPA of C3 lies at an oblique angle to the jet. At 273 GHz, Nartallo et al. (1998) have measured a slowly increasing EVPA, starting at  $116^\circ$  in 1992.81 and ranging up to  $139^\circ$  for their last measurement (1995.9). This increase is coincident with a slow rise in total millimeter flux density during this interval (Reuter et al. 1997; Tornikoski et al. 1996).

The integrated polarization EVPA measurements of this source by the University of Michigan group at 14.5 GHz show large fluctuations between  $60^\circ < \chi < 170^\circ$  since

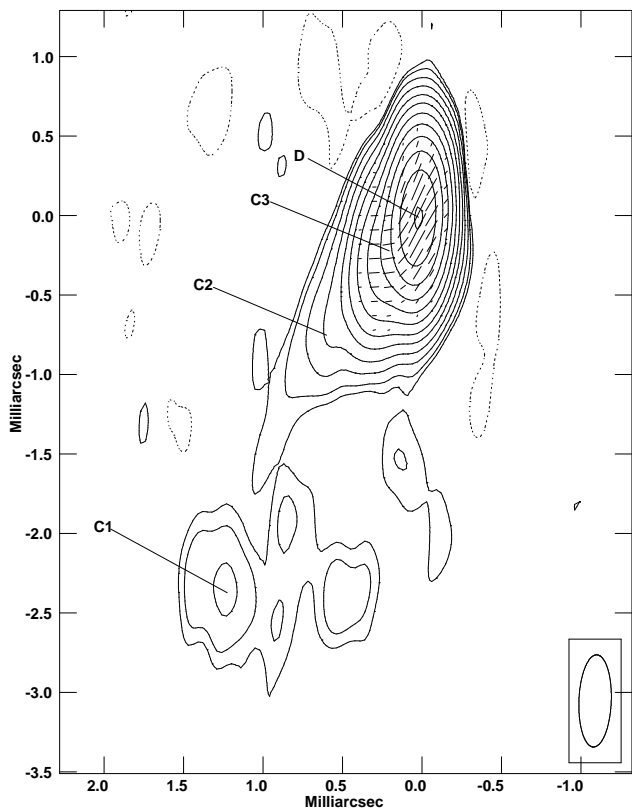


FIG. 5.—VLBA total intensity image of 1334–127 at 43 GHz, epoch 1996.90, with electric polarization vectors superimposed. Contours are  $-0.06\%$ ,  $0.06\%$ ,  $0.1\%$ ,  $0.2\%$ ,  $0.4\%$ ,  $0.8\%$ ,  $1.5\%$ ,  $3\%$ ,  $6\%$ ,  $12\%$ ,  $24\%$ ,  $48\%$ , and  $96\%$  of the peak brightness,  $9.362 \text{ Jy beam}^{-1}$ . The polarization vectors are scaled such that  $1 \text{ mas} = 1.856 \text{ Jy beam}^{-1}$ .

1993.5. There is an overall trend during flares for the EVPA angle to increase (i.e., become more parallel to the jet) as the total fractional polarization increases, perhaps because of the transverse magnetic field alignments of new components (see § 4). In the case of 1334–127, it is impossible to test this hypothesis using a single-epoch map, since we cannot ascertain the apparent speed or birth date of component C3. The nonaligned EVPA and fractional polarization of C3, however, would suggest that it would affect the total (single-dish) EVPA. A concurrent (epoch 1996.93) 14.5 GHz EVPA measurement of  $95.3 \pm 3^\circ$  made by the University of Michigan group supports this scenario. The EVPA of the core (D), being highly aligned with the jet, would appear to indicate that a new component is present, below the resolution of our image. The University of Michigan 14.5 GHz data do show a sudden  $\sim 80^\circ$  increase in EVPA beginning in 1997.0 (1 month after these observations), which was accompanied by a slight (1%) increase in  $m$ .

### 3.1.4. 1514–241 (AP Librae)

AP Lib is a low-redshift ( $z = 0.0486$ ) BL Lac object with rapidly variable optical flux (night-to-night; Carini et al. 1991) and optical polarization as high as  $8.0\%$  (Stickel, Meisenheimer, & Kühr 1994). Tornikoski et al. (1993) measured a flat radio spectrum out to  $\sim 40$  GHz, followed by an  $\alpha \simeq -0.3$  falloff toward the infrared/optical region. No gamma rays have been detected from this BL Lac object by either EGRET or the Whipple telescope (Weekes et al. 1996). At arcsecond scales, AP Lib displays a straight radio jet extending at least  $20''$  to the east of the core at P.A.  $\simeq 88^\circ$

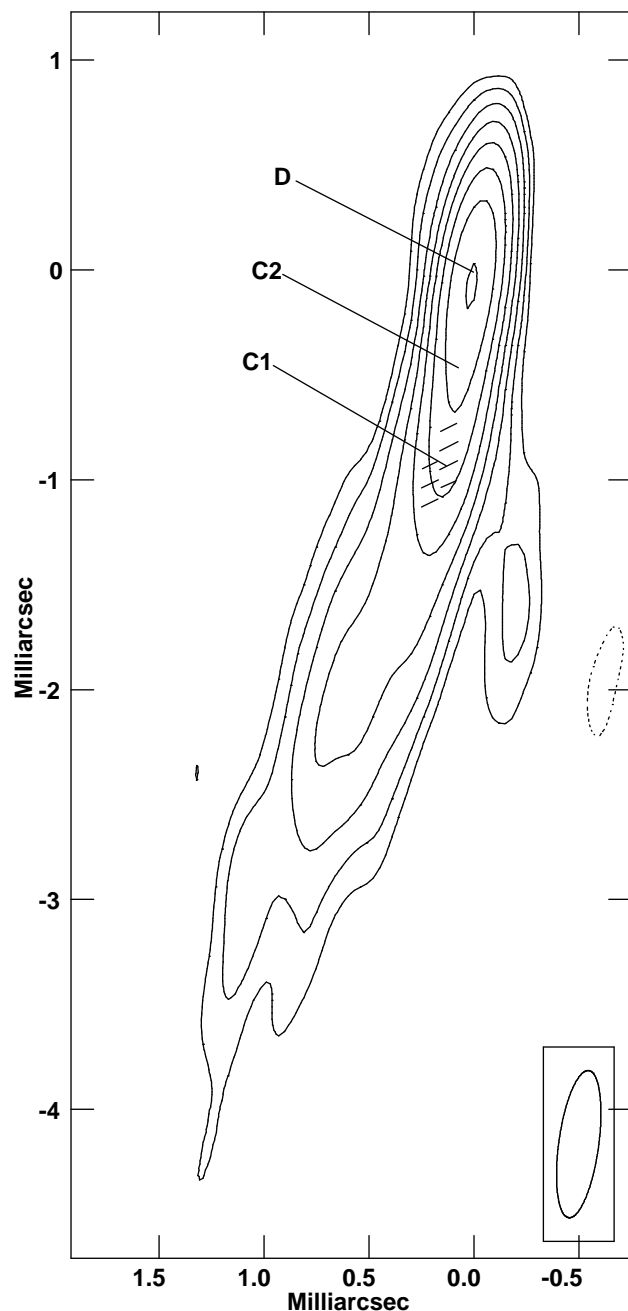


FIG. 6.—VLBA total intensity image of AP Librae (1514–241) at 43 GHz, epoch 1996.90, with electric polarization vectors superimposed. Contours are  $-0.75\%$ ,  $0.75\%$ ,  $1.5\%$ ,  $3\%$ ,  $6\%$ ,  $12\%$ ,  $24\%$ ,  $48\%$ , and  $96\%$  of the peak brightness,  $815 \text{ mJy beam}^{-1}$ . The polarization vectors are scaled such that  $1 \text{ mas} = 185 \text{ mJy beam}^{-1}$ .

(Morganti, Killeen, & Tadhunter 1993; Antonucci & Ulvestad 1985), and observations by Bondi et al. (1996) show extended emission out to  $57''$ .

Because of the southern declination of AP Lib, the resolution beam of the VLBA is highly elongated, and unfortunately extended in nearly the same direction as the parsec-scale jet. As a result, the brightness distribution in Figure 6 is highly smoothed. Within  $\sim 1 \text{ mas}$  of the core, the jet is fairly straight at P.A.  $\simeq 171^\circ$  and contains two components (C1 and C2; see Table 2). The jet then bends through  $14^\circ$  to P.A.  $\simeq 157^\circ$ . Since no other VLBI maps of this source have been published in the literature, the apparent velocities of these components cannot be estimated.

At 43 GHz, we detect polarized emission only at the location of component C1, where the fractional polarization is approximately 7%. The electric vector of C1 lies at an oblique angle to the local jet direction. The upper limit on the core polarization of AP Lib is 0.8%, which is somewhat lower than the other blazar cores in our sample. If this is a result of Faraday depolarization caused by dense nuclear gas (e.g., Cawthorne et al. 1993), it would have to be extremely localized (within  $\sim 0.6 h^{-1} \text{ csc } \theta \text{ pc}$  of the core), given the fractional polarization of component C1. On the other hand, it is possible that the core is merely in a low-polarization state in which it is not creating any new components. The centimeter-wave EVPA (from the University of Michigan data) has been relatively stable since 1994.5 ( $10^\circ \lesssim \text{EVPA} \lesssim 55^\circ$ ), and no major polarized or total intensity outbursts have occurred since that time at these wavelengths. Nartallo et al. (1998) have made one measurement of the EVPA at 273 GHz (epoch 1993.15), and obtained  $4.1 \pm 8^\circ$ . These data are consistent with a transverse  $B$  field during a period of rising 230 GHz flux density (Tornikoski et al. 1996).

### 3.2. Calibrator Sources

In this section we discuss the high-resolution morphology and polarization properties of four calibrator sources. With

the exception of DA 193, these sources have all been the subject of other recent studies at a variety of wavelengths. Our discussion will thus concentrate on new information regarding these sources that derive from our 43 GHz observations.

#### 3.2.1. DA 193 (0552+398)

The low-polarization quasar DA 193 has a classical homogeneous synchrotron self-absorption spectrum, with a turnover at 5 GHz (Spangler, Mutel, & Benson 1983). It has been classified as a GHz-peaked spectrum source (GPS) by O'Dea, Baum, & Stanghellini (1991), and is the only non-blazar in our sample.

DA 193 has been shown to be extremely compact on both arcsecond (Dallacasa et al. 1995; Stanghellini et al. 1990) and milliarcsecond (Fey et al. 1996) scales. The superior resolution of our 43 GHz image (Figs. 7 and 8), however, reveals a complex source structure. When considered together with the polarized intensity distribution, there appear to be at least four possible components in the core region of this source, as well as a short jet extending to the west. The slight extension to the east may be a counterjet, but is more likely to be the core (D), since previous VLBI images taken by Spangler et al. (1983), Charlot (1990), and Bajkova, Pyatunina, & Finkelstein (1996) show no structure

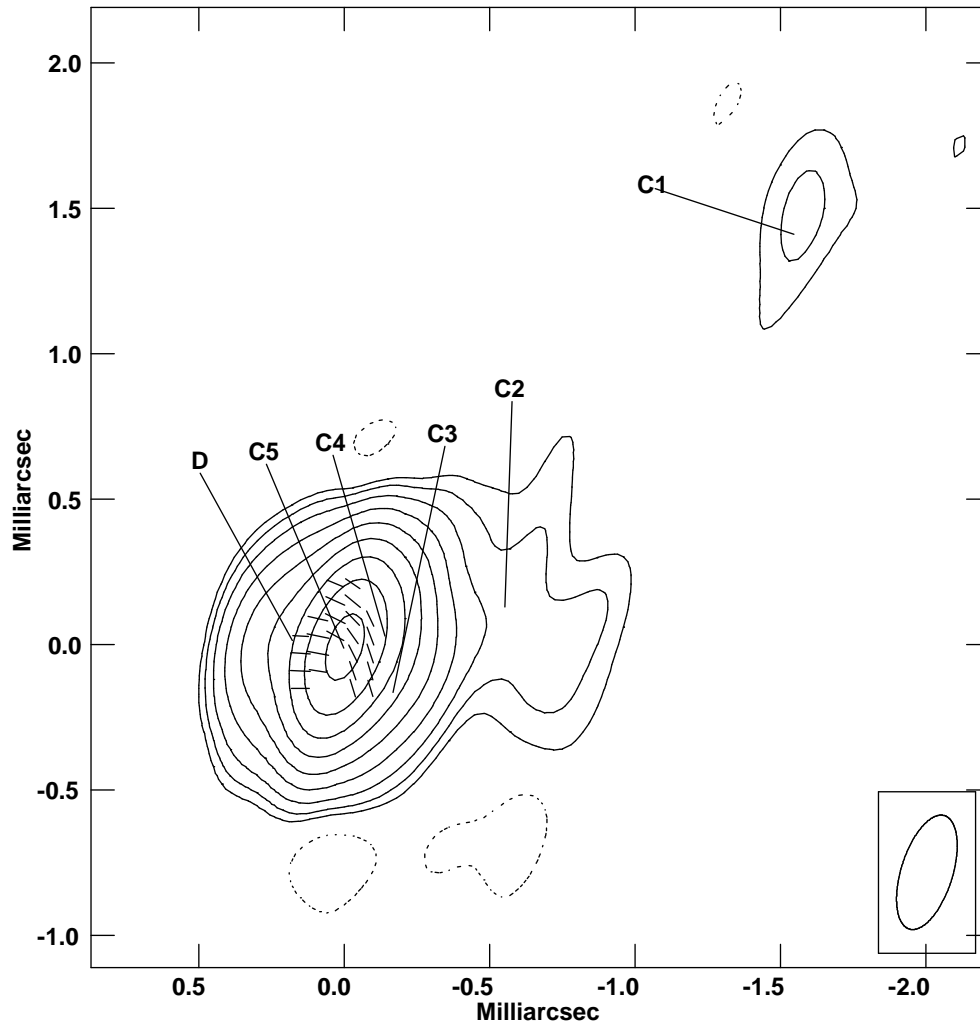


FIG. 7.—VLBA total intensity image of DA 193 (0552+398) at 43 GHz, epoch 1996.90, with electric polarization vectors superimposed. Contours are  $-0.3\%$ ,  $0.3\%$ ,  $0.6\%$ ,  $1.2\%$ ,  $2.5\%$ ,  $5\%$ ,  $10\%$ ,  $20\%$ ,  $40\%$ , and  $80\%$  of the peak brightness,  $1.849 \text{ Jy beam}^{-1}$ . The polarization vectors are scaled such that  $1 \text{ mas} = 247 \text{ mJy beam}^{-1}$ .

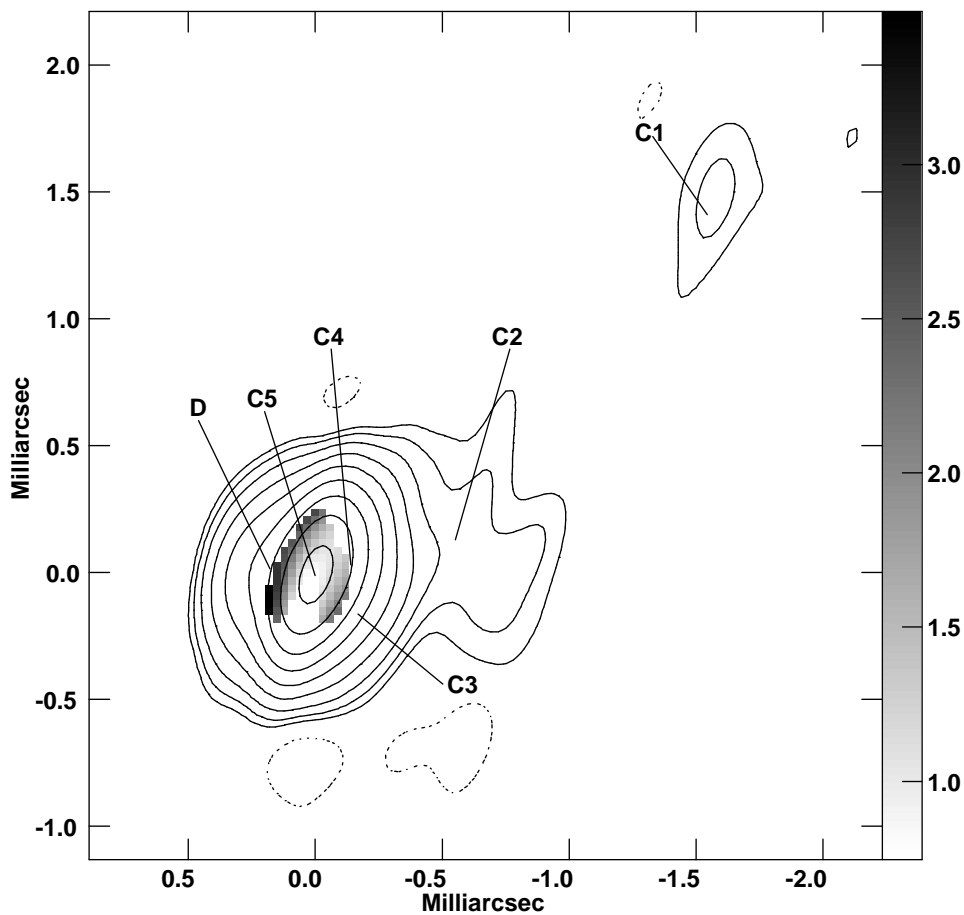


FIG. 8.—VLBA total intensity image of DA 193 (0552+398) at 43 GHz, epoch 1996.90, with contours as in Fig. 7. The linear gray scale corresponds to fractional polarization in percent.

in this direction. A weak core at this position is consistent with the low self-absorption turnover frequency, which implies that the core is either misdirected or relatively inactive.

Bajkova et al. (1996) found a proper motion of  $0.03 \pm 0.01$  mas yr<sup>-1</sup> for component C2, based on three epochs at  $\sim 8$  GHz (1981.5, 1985.37, and 1994.9). The position of C2 in our 43 GHz image is consistent with this  $\mu$  value, taking into account a possible shift in core position attributable to observing frequency (see Lobanov 1998). At the source redshift of  $z = 2.365$ , the proper motion corresponds to an apparent velocity of  $2.2 \pm 0.7 h^{-1} c$ . The presence of superluminal motion in this object is of interest, because the jets of GPS sources generally show very little or no proper motion (Vermeulen & Cohen 1994). We speculate that DA 193 may be similar to 4C 39.25 (Alberdi et al. 1997), with the jet misdirected at the core but pointed almost directly along the line of sight farther downstream.

Our polarization image of DA 193 resolves two regions of nearly orthogonal polarization on either side of C5. A partial cancellation of polarized flux from these two components may be responsible for the low polarized flux density at the location of C5. The EVPA in the eastern polarized region (near D) is parallel to the local jet direction defined by D, C4 and C5, while that of the western region is at an oblique angle. Higher resolution polarization observations are needed to clarify the structural details of the inner jet in this source.

The integrated fractional polarization of the inner 0.5 mas of DA 193 is rather low ( $\sim 2\%$ ). This may partly be due to Faraday depolarization, since very high ( $> 4700$  rad m<sup>-2</sup>) rest-frame rotation measures have been measured for this source (Junor et al. 1996; O’Dea et al. 1990).

Our data also suggest a very weak extended component located 2.3 mas to the northwest of D. This component, labeled C1 in Table 2, was not detected by previous studies, and if real would indicate a substantial curvature in the jet. Bajkova et al. (1996) detected a component with a similar P.A. ( $-58^\circ$ ) in their epoch 1994.9 map at  $r = 1.19$  mas, but it is not likely that this was C1, since this would imply an excessively large proper motion of  $0.55$  mas yr<sup>-1</sup> ( $\approx 40 h^{-1} c$  for  $q_0 = 0$ ).

### 3.2.2. OJ 287

OJ 287 is a well-studied BL Lac object at  $z = 0.306$  that displays extremely large and rapid flux variations at both radio and optical wavelengths. We discuss the milliarcsecond-scale polarization structure of OJ 287 only; the total-intensity VLBI properties of this source at 43 GHz are presently under investigation by Marscher & Marchenko (1997).

The 43 GHz total-intensity image of OJ 287 is presented in Figure 9. The EVPA starts out at  $-119^\circ$  near the core, and changes to  $-108^\circ$  at  $r \sim 0.1$  mas, suggesting the existence of a component very close to the core. Indeed, our Gaussian-component fit gives a component (C6) at  $r = 0.12$

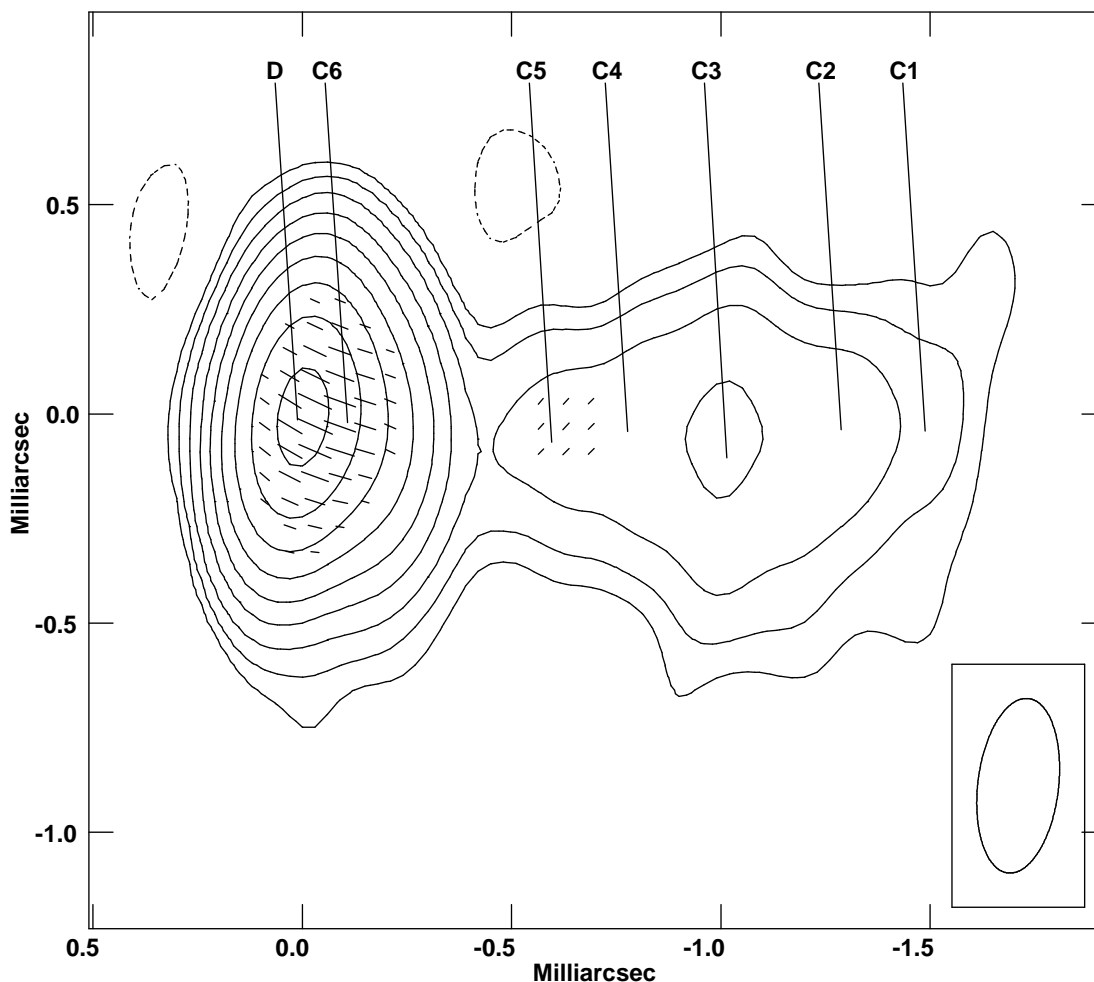


FIG. 9.—VLBA total intensity image of OJ 287 at 43 GHz, epoch 1996.90, with electric polarization vectors superimposed. Contours are  $-0.3\%$ ,  $0.3\%$ ,  $0.6\%$ ,  $1.2\%$ ,  $2.5\%$ ,  $5\%$ ,  $10\%$ ,  $20\%$ ,  $40\%$ , and  $80\%$  of the peak brightness,  $1.254 \text{ Jy beam}^{-1}$ . The polarization vectors are scaled such that  $1 \text{ mas} = 372 \text{ mJy beam}^{-1}$ .

mas. The polarized emission from these components is blended together.

At distances greater than  $\sim 0.5 \text{ mas}$  from the core, the emission is in the form of a diffuse jet, and our Gaussian model fit is somewhat uncertain. We identify five possible components, of which only one (C5;  $r = 0.61 \text{ mas}$ ) has associated polarized emission. A 22 GHz image taken in 1995.9 by (A. Alberdi 1997, private communication) shows a component with a similar EVPA ( $-32^\circ$ ) at  $r = 0.32 \text{ mas}$ .

The fractional polarization of C5 is quite high ( $\sim 36\%$ ) compared to C3, which is at least 4 times as bright in total intensity. Given the noise level in the image, the fractional polarization of C3 must be  $\lesssim 19\%$ . The jet of OJ 287 appears to have a variety of magnetic field orientations, which is also reflected in the lack of a preferred polarization position angle for its core. The data of Marscher & Marchenko (1997) suggest that the evolution of components in this object is both rapid and complex, and can only be studied with frequently sampled ( $\sim$  bimonthly) VLBA observations.

### 3.2.3. 3C 279

3C 279, an extremely bright, gamma-ray-loud (Fichtel et al. 1994) OVV quasar with  $z = 0.538$ , performed an important role as an EVPA calibrator in this study (see § 2), owing

to its bright component (C4) with an EVPA parallel to the jet.

In our 43 GHz image (Fig. 10), we detect component C5, which has been shown to remain stationary for the past several years (Leppänen et al. 1995; Wehrle et al. 1998). Our measured core separation ( $1.19 \text{ mas}$ ) is slightly higher than previously reported values ( $1.17 \text{ mas}$ ; Leppänen 1995), but we suspect that this is the result of a shift in the apparent core position owing to our higher observing frequency.

Leppänen et al. (1995) detected two components, C6 and C7, at separations of  $0.33$  and  $0.10 \text{ mas}$ , respectively, in their epoch 1994.33 image. We are not able to make reliable identifications of these components in our 43 GHz image, however, since the jet appears to be nearly continuous for  $r \lesssim 1 \text{ mas}$ .

The polarization vectors in the image of 3C 279 (Fig. 10) reveal a strong polarized flux in the core region, with EVPAs varying between  $-115^\circ$  and  $-118^\circ$ . These line up well with the position angle of C4. The latter component has remained strongly polarized ( $m \sim 15\%$ ), despite its large projected separation of  $13.3h^{-1} \text{ pc}$  from the core. The total-intensity and polarized-emission peaks of C4 lie at a different position angle from that of the inner jet, and past VLBI observations have shown that it has remained steadily on the same trajectory (P.A. =  $-115^\circ$ ) since 1989 (Carrara et

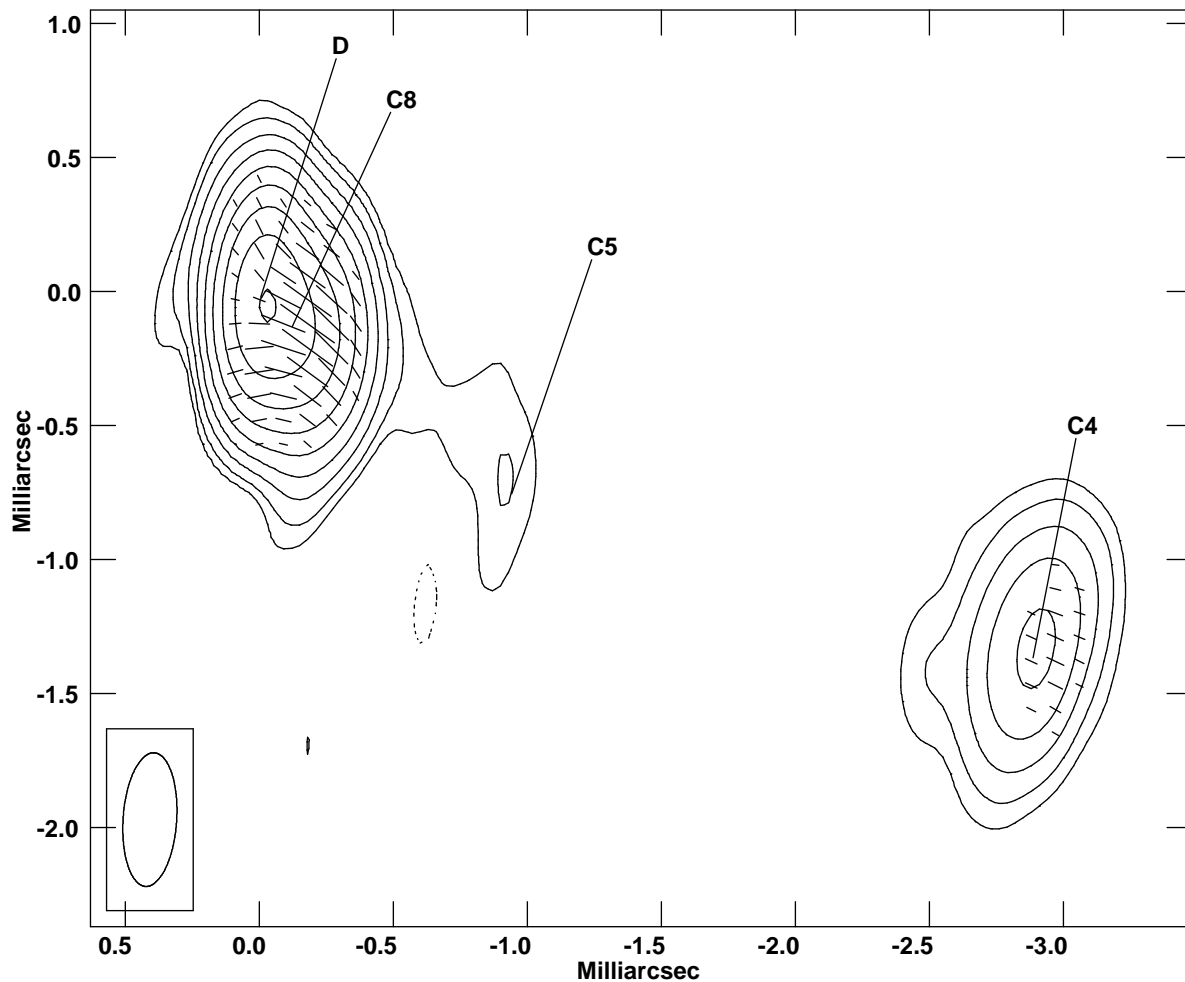


FIG. 10.—VLBA total intensity image of 3C 279 at 43 GHz, epoch 1996.90, with electric polarization vectors superimposed. Contours are  $-0.35\%$ ,  $0.35\%$ ,  $0.7\%$ ,  $1.5\%$ ,  $3\%$ ,  $6\%$ ,  $12\%$ ,  $24\%$ ,  $48\%$ , and  $96\%$  of the peak brightness,  $13.232 \text{ Jy beam}^{-1}$ . The polarization vectors are scaled such that  $1 \text{ mas} = 2.475 \text{ Jy beam}^{-1}$ .

al. 1993). The polarized emission peak lies  $\sim 0.07 \text{ mas}$  farther from the core than the total intensity peak (Fig. 11). Leppänen et al. (1995) found a similar occurrence for the stationary component C5, which they determined to have an inferred magnetic field parallel to the jet.

Lower-resolution (5 GHz) VLBI maps of 3C 279 at an earlier epoch (1987.4) by Cawthorne & Gabuzda (1996) show a remarkably different magnetic field configuration in the milliarcsecond-scale jet. Their components C2 and C3 both had magnetic fields aligned parallel to the jet, and were located at  $r = 4.4$  and  $r = 2.9 \text{ mas}$ , straddling the present (1996.9) location of C4, which has a *perpendicular*  $\mathbf{B}$  field. It is interesting that such strongly polarized components going by the same point in the jet have such different field configurations. Cawthorne et al. (1993) have suggested that in situations where the  $\mathbf{B}$  field of the underlying jet is strongly longitudinal, a weak shock may increase both the total intensity and the transverse field component, yet reduce the total fractional polarization. This results from a cancellation of the polarized emission from the two orthogonal  $\mathbf{B}$ -field components. Such a scenario may be occurring for component C4. Under this interpretation, the aligned EVPAs and higher fractional polarizations of components C2 and C3 (15% and 24%, respectively) might result from the fact that they represent weaker shocks that do not sufficiently change the underlying EVPA of the jet.

### 3.2.4. 1611 + 343

Although this  $z = 1.401$  quasar has low optical polarization (1.7%; Impey & Tapia 1990), it displays characteristics typical of the blazar class. It is gamma-ray loud (Sreekumar et al. 1996), displays superluminal motion (Piner & Kingham 1997, hereafter PK97), and has OVV-like flux density variations (Tornikoski et al. 1994).

PK97 have recently completed an extensive VLBI study of this quasar at 8 GHz, and find several components with superluminal velocities in the range  $3.8 h^{-1} < \beta_{\text{app}} < 11.5 h^{-1}$  moving outward from the core with different trajectories. Our higher resolution 43 GHz image (Fig. 12) allows a check on the component identifications made by PK97. We use the same nomenclature as PK97 wherever possible in Table 2.

Starting farthest from the core, their component C1 is not present on our image, as was the case in their epoch 1996.24 map. There is some difficulty in assigning a definite identification to C2 ( $r \sim 3 \text{ mas}$ ), because the jet is fairly continuous in this region. Component C3 is well defined in our image, and appears to have the least scatter in PK97's diagram of separation versus time. These authors measured a best-fit slope of  $\mu = 0.23 h^{-1} \text{ mas yr}^{-1}$ , which gives an apparent speed of  $\beta_{\text{app}} = 10.8 h^{-1}$ . There is a region of very weak polarized flux  $\sim 0.1 \text{ mas}$  to the south of C3, with an EVPA

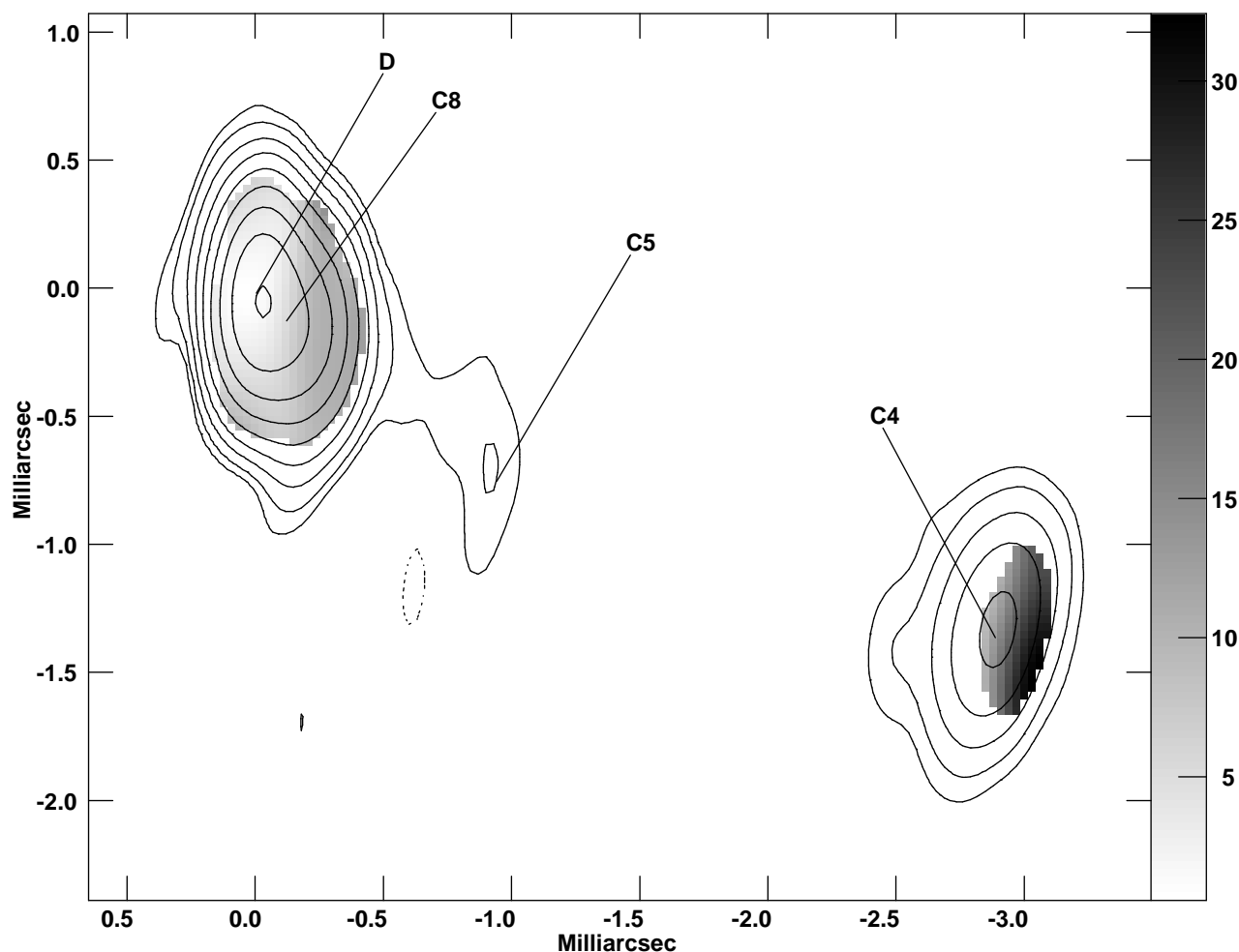


FIG. 11.—VLBA total intensity image of 3C 279 at 43 GHz, epoch 1996.90, with contours as in Fig. 10. The linear gray scale corresponds to fractional polarization in percent.

that points to the diffuse jet region near C2. This polarized region may be associated with a stationary, weak, oblique shock that alters the jet direction at this point.

There is no component C4 at the predicted separation ( $r = 1.7$  mas) for this epoch, given the apparent speed derived by PK97. It is possible that C4 has blended into C3, since there is a slight extension to the north of the latter component. PK97 also report the detection of a component C5 at  $r = 0.63$  mas in their epoch 1996.24 map, which is not apparent in Figure 12. We instead measure a component C5a at  $r = 1.38$  mas.

A Gaussian model fit to the core region of the total intensity image yields three components: D, C7, and C6. The polarization image shows a core EVPA of  $\sim 94^\circ$ , roughly perpendicular to the local jet direction, while the EVPA at the position of C6 is at a more oblique angle ( $125^\circ$ ).

#### 4. OVERALL PROPERTIES OF THE BLAZAR SAMPLE

In this section we discuss the general polarization properties of our blazar sample. The source DA 193 will not be included in this discussion, since it is a low optical polarization, non-OVV quasar classified as a GPS source by O’Dea et al. (1991). While the remaining sources were not selected using any well-defined criteria apart from strong, core-dominated flux density, they are grouped together here based on their common blazar characteristics.

#### 4.1. Blending and Opacity Effects in the Core

The term “core” in VLBI studies is often used loosely to describe a strong, unresolved, stationary, flat-spectrum component at the base of the jet, from which other moving components appear to emerge. Its characteristics, however, are highly dependent on observing frequency and resolution. The flat spectrum of the core region is thought to result from the superposition of many distinct synchrotron-emitting regions that lie along the jet, those closer to the core having spectra peaked at higher frequencies. When this region is smeared out by a large beam at lower frequencies, the position of peak emission (the “core”) appears to shift outward with decreasing observing frequency. This is a well-documented effect (see Lobanov 1998) that is caused by the nature of the core at low frequencies, according to Blandford & Königl (1979), who identify it with the  $\tau \sim 1$  part of the ambient jet.

In general, the beam size of VLBA images is much larger than the structural scale of the inner jet, which also affects the observed polarization properties of the core. Long-term monitoring of the integrated polarization at centimeter wavelengths (Aller et al. 1985) has shown that in many cases sources have stable EVPAs, but lose this tendency during periods of high flux variability. Gabuzda et al. (1994) find evidence that in BL Lac objects, the natural polarization state of the core is such that the electric field is perpendicu-

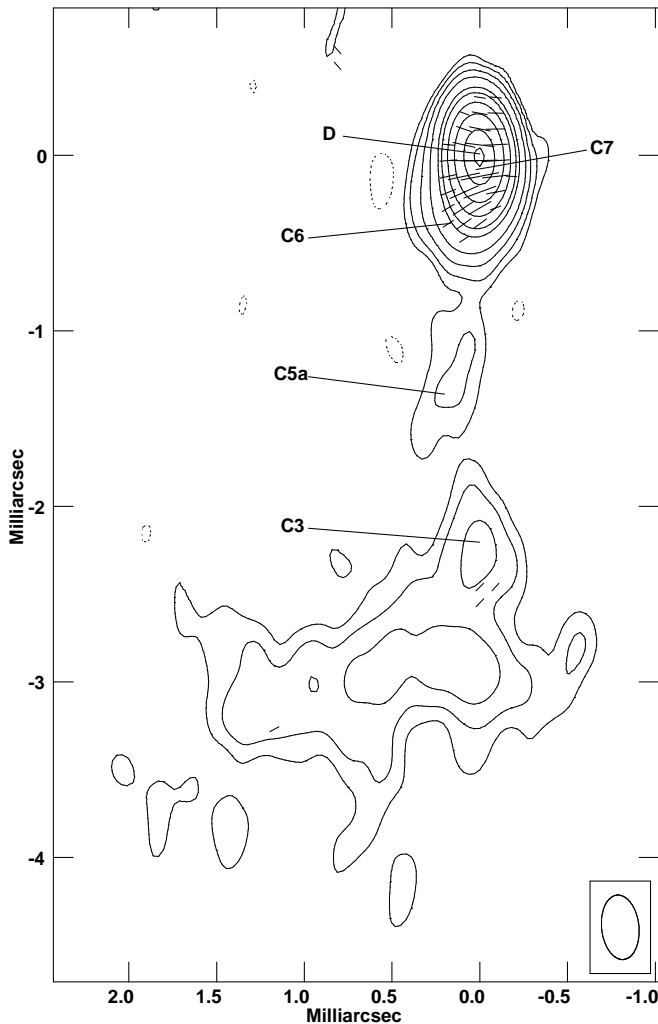


FIG. 12.—VLBA total intensity image of 1611+343 at 43 GHz, epoch 1996.90, with electric polarization vectors superimposed. Contours are  $-0.25\%$ ,  $0.25\%$ ,  $0.5\%$ ,  $1\%$ ,  $2\%$ ,  $4\%$ ,  $8\%$ ,  $16\%$ ,  $32\%$ ,  $64\%$ , and  $95\%$  of the peak brightness,  $2,910 \text{ Jy beam}^{-1}$ . The polarization vectors are scaled such that  $1 \text{ mas} = 372 \text{ mJy beam}^{-1}$ .

lar to the local jet direction. If a new component with a sufficiently strong perpendicular magnetic field component emerges from the core (below the resolution level of VLBI techniques), the EVPA will undergo a rapid change, becoming parallel to the jet. Therefore, at any given time for a particular source, it is unclear whether the observed EVPA is related to the true magnetic field orientation of the core or heavily influenced by one or more emerging components.

The observed polarization structure is also strongly affected by blending, to a much larger degree than the total intensity structure. In Stokes  $I$  images, the flux from closely spaced components adds linearly, while in polarization-sensitive images, emission from such regions can be cancelled out, provided that their EVPA orientations are nearly orthogonal. This effect is seen in the inner jet of DA 193 (§ 3.2.1). At lower resolution levels, very little polarized emission would be detected from the latter source, as we have verified by convolving our map with a larger beam. The effects of blending can therefore cause erroneous measurements of core fractional polarization, and caution must be exercised when comparing values obtained at different observing frequencies, which generally have different beamwidths.

#### 4.2. Electric Vector Orientation of Core Components

The position angle difference between the EVPA of the core and the inner jet direction provides an indicator of the magnetic field configuration in this region. Gabuzda et al. (1994) have plotted this quantity at centimeter wavelengths for a sample of BL Lac objects, and find a bimodal distribution, with peaks at  $0^\circ$  and  $90^\circ$ . They interpret this as a temporal selection effect caused by the blending of new components emerging from the core, as discussed in § 4.1. The same bimodal distribution has not been seen for quasars, suggesting that the inner magnetic field configurations are somehow different in these two classes of object (Cawthorne et al. 1993).

In Figure 13, we present the distribution of  $|\chi_{\text{core}} - \theta_{\text{mas}}|$  for our sample, where  $\chi_{\text{core}}$  is the core EVPA and  $\theta_{\text{mas}}$  is the structural positional angle of the jet. We define the latter quantity as the position angle of the innermost jet component in our maps. With the exception of 1611+343, all the sources in our sample have core EVPAs nearly parallel to the jet. The relatively small number of objects makes it impossible to conclude whether this is merely coincidence (i.e., given their high degree of variability, all may be undergoing birth of a new component), or whether higher resolution polarization images are revealing a previously unseen region of strongly ordered magnetic field near to the core. We note that only three other AGNs have had polarization images published at this frequency (0420-014 and 3C 454.3, Kembal et al. 1996; 3C 120, Gómez et al. 1998), and all have aligned EVPAs.

We find no apparent differences in the core polarization properties of the BL Lacs and quasars in our sample, which is consistent with the findings of the single-dish blazar study by Nartallo et al. (1998) in the millimeter/submillimeter-wave regime. The latter authors found a tendency for blazars with high millimeter-wave fractional polarization to have EVPAs aligned with the jet, while the low-polarization objects preferentially had perpendicular orientations. In addition, Tornikoski et al. (1993) have found marked differences in the variability properties of high and low optical polarization quasars, with the low-polarization objects showing a much lower degree of variability. Interestingly, the only core with a perpendicular EVPA in our sample (the quasar 1611+343) is also the only object with low optical polarization. These findings suggest that the inner jet properties of beamed AGNs at centimeter/millimeter wavelengths may be closely related to their degree of polarization at higher frequencies.

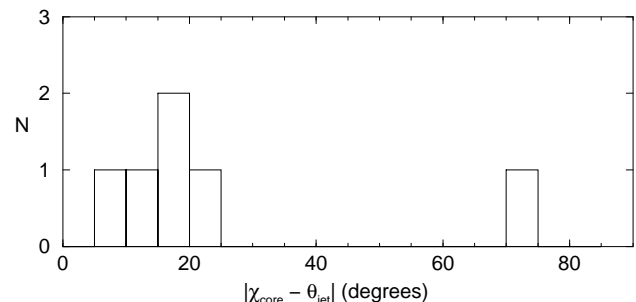


FIG. 13.—Distribution of offset between electric vector position angle and local jet direction for all of the cores in our sample with detected polarization. The EVPAs are predominantly parallel to the jet, with the exception of the low optical polarization quasar 1611+343.

#### 4.3. Polarization Properties of Jet Components

Because of the limited dynamic range of our “snapshot” VLBA observations, we were unable to detect any significant polarized emission from the underlying jets in our sample. We did, however, detect a moderate number of highly polarized knots. In several cases, the peak of the polarized emission was somewhat offset from the total intensity peak (e.g., component C4 in 3C 279). This phenomenon was also detected in several blazars at 22 GHz by Leppänen et al. (1995), and may provide important constraints on physical models for these knots. A common interpretation (e.g., Hughes et al. 1985) is that these features are associated with plasma that has been compressed as a result of a shock front that is perpendicular to the jet flow (in the rest frame of the shock). Laing (1980) has shown that for the downstream (shocked) plasma, the parallel component of an originally tangled magnetic field is greatly enhanced, while the component perpendicular to the shock front remains unchanged. Since the beamwidth of VLBI maps is expected to be much larger than the width of this compressed slab of plasma, the observed electric polarization vector for a strong shock will be perpendicular to the slab and aligned with the jet axis.

Cawthorne et al. (1993) have suggested that these types of slabs (also called “Laing sheets”) are responsible for the alignment of the electric vectors with the jet in BL Lac objects. Quasars, on the other hand, have weaker shocks and/or a stronger underlying longitudinal magnetic field. This interpretation appears to be consistent with the distribution of  $|\chi_{\text{jet}} - \theta_{\text{mas}}|$  for the Pearson-Readhead AGN sample at 5 GHz (Cawthorne et al. 1993). It is unclear, however, whether this relation holds at higher frequencies that probe jet regions closer to the core.

In Figure 14 we show the distribution of  $|\chi_{\text{cpt}} - \theta_{\text{jet}}|$  for all the polarized components seen in our images (*shaded regions*), along with those of all other blazars (3C 273, 3C 279, and 3C 345, Leppänen 1995; 3C 454.3, Kembell et al. 1996; OJ 287, A. Alberdi 1997, private communication) that have been imaged to date with the VLBA in cross-polarization mode at 22 GHz or higher. Although this is not a complete sample, the sources in Figure 14 all display blazar properties. The distribution does contain several components with aligned EVPAs ( $|\chi_{\text{cpt}} - \theta_{\text{jet}}| \simeq 0$ ), but the majority of the components have oblique EVPAs that are not easily reconcilable with the transverse shock model. It is possible that the EVPAs of these components may be

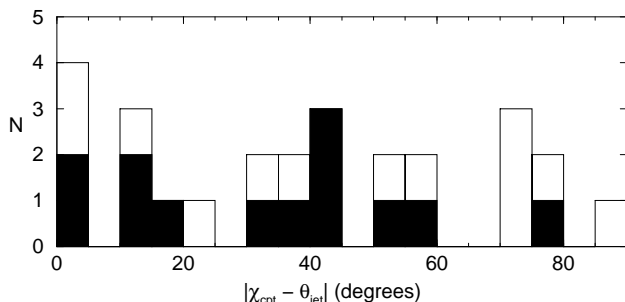


FIG. 14.—Distribution of offset between electric vector position angle and local jet direction for all of the polarized components seen in our sample images (*shaded areas*), along with those of all other sources imaged to date with polarization-sensitive VLBI at frequencies  $\geq 22$  GHz.

affected by varying degrees of Faraday rotation, but this is not likely to be a strong effect. First, the amount of Faraday rotation is greatly reduced at these high observing frequencies. Second, the high-frequency polarization images of these and other AGNs show that the innermost jet components tend to have better-aligned EVPAs, despite that fact that more Faraday-screening gas would be expected close to the base of the jet. Finally, Gabuzda & Cawthorne (1996) have found that the core polarizations of nine BL Lacs were in fact slightly *higher* at 5 GHz than at 8.3 GHz, which cannot be explained by Faraday depolarization.

It is also possible that the local jet directions may have been estimated incorrectly, owing to small-scale jet bending below the resolution level of the images. If recent helical jet models applied to such sources as 3C 345 (Steffen et al. 1995), OJ 287 (Vicente, Charlot, & Sol 1996), and MK 501 (Conway & Wrobel 1995) are correct, then abrupt changes in position angle are to be expected at certain points along the jets of blazars, as a consequence of projection effects. A strong test of these helical models would be to monitor the EVPAs of components moving down a jet, and look for correlations with their apparent trajectories. It is unlikely that all the misaligned EVPAs in Figure 14 can be attributed to helical geometries, however, because in most cases the jet shows no sign of bending near the misaligned component. In the next section we investigate whether these observed EVPA misalignments might instead be due to nontransverse (oblique) shocks.

#### 5. OBLIQUE SHOCK MODEL

The concept of shock fronts lying at intermediate angles to the jet axis has already been applied successfully to several AGNs. For example, Bicknell & Begelman (1996) have recently developed a model for M87 in which oblique shocks are generated as a result of helical Kelvin-Helmholtz instability modes in the jet. Oblique shocks in sheaths have also been used by several authors (Lind & Blandford 1985; CC90) to model conical shocks. The observed polarization vectors of conical shock structures, however, are always either perpendicular or parallel to the jet axis because of symmetry (CC90), and cannot explain the observed component EVPA misalignments above 22 GHz.

On the other hand, the EVPA of a single moving oblique shock can take on a variety of orientations, depending on the position of the observer. Although the details of how moving oblique shocks form in three-dimensional jet flows are not yet well understood, recent numerical jet simulations suggest that transverse shocks often evolve into oblique shocks as a result of nonuniform shear around their perimeters (D. A. Clarke 1998, private communication). Oblique shocks are known to deflect the flow of the jet (Königl 1980) either upstream, in the case of a forward shock, or downstream, in the case of a reverse shock. These structures may produce small wiggles in the jet axis up- or downstream, the amplitudes of which would depend on the lifetime and other parameters associated with the shock. We will not discuss the dynamical evolution of these structures in this paper, however, since we will show that the observed component EVPA misalignment distribution in blazars cannot be fitted by a single population of oblique shocks having arbitrary inclinations with respect to the jet axis.

We begin by extending the model of CC90, who derived expressions for the EVPA, fractional polarization, and total polarized intensity of a stationary, oblique shock of arbi-

trary orientation. We generalize their model to include moving shocks by adopting appropriate limits to the velocity of the upstream gas and the shock obliquity. Here we assume the gas to have an extreme relativistic equation of state on both sides of the shock front, and that the upstream flow is parallel (nonexpanding) and contains a randomly oriented magnetic field.

To ensure consistency with CC90, we perform appropriate Lorentz transformations of the relevant angles and velocities to obtain quantities in the rest frame of the moving shock. The details of these transformations are presented elsewhere (Lister 1998).

Let us imagine a relativistic jet with upstream flow velocity  $\beta'_u$  in the observer frame, oriented at a viewing angle  $\theta'$  (measured between the observer vector  $k'$  and  $\beta'_u$ ). A shock with arbitrary inclination angles  $\eta$  and  $\phi$  moves down the jet at a speed  $\beta'_s$ . Following the nomenclature in Figure 1 of CC90, we take  $\eta$  to represent the angle between the plane of the shock front and the jet axis. The angle between the plane containing the up- and downstream velocities and the  $k$ - $\beta_u$  plane is equal to  $\phi$ . The unprimed quantities here refer to those measured in the rest frame of the shock.

Since the oblique shock model of CC90 is valid only for upstream velocities greater than the relativistic sound speed ( $c/3^{1/2}$ ), the Lorentz transformation between the observer and shock frames implies a maximum shock velocity in the observer frame of

$$\beta'_{s,\max} = \frac{\beta'_u - 1/\sqrt{3}}{1 - \beta'_u/\sqrt{3}}. \quad (1)$$

There is also a limited range of obliquity for which the model is valid (see eq. [5] of CC90):

$$\sin \eta > (\sqrt{2}\Gamma_u \beta_u)^{-1}. \quad (2)$$

We have developed a Monte Carlo simulation that generates a population of 1000 jets, each with an oblique shock of the type described above. The sources in each simulation all have identical upstream Lorentz factors  $\Gamma'_u$  and flat spectral indices ( $\alpha = 0$ ), such that the continuous (jet) emission is boosted by a factor of  $\delta^2$  in the observer frame. The probability distribution of viewing angles for a flux-limited sample of such jets is given by Vermeulen & Cohen (1994):

$$p(\theta')d\theta' = \frac{a\beta'_u(1 - \beta'_u \cos \theta')^{-a-1} \sin \theta'}{(1 - \beta'_u)^{-a-1}} d\theta', \quad (3)$$

where  $a = 2$  for  $q_0 = 0$ .

For each shock, we assign a random velocity  $\beta'_s$  between 0 and  $\beta'_{s,\max}$ , and random angles  $\phi$  and  $\eta$  in the rest frame of the shock front. The last quantity is distributed between  $\eta_{\min}$  and  $90^\circ$ , with a probability distribution of  $p(\eta) \propto \sin \eta$ , where  $\eta_{\min}$  is given by equation (2). A spectral index of  $\alpha = -0.5$  is used for all shocks. The predicted EVPAs ( $\chi$ ) and fractional polarizations ( $m$ ) are calculated, and any generated shocks with  $m < 1\%$  are excluded from the final sample. This is done in order to simulate the limited sensitivity of VLBA polarization images. Our conclusions are not sensitive to the exact value of this cutoff.

The predicted distributions of  $|\chi - \theta_{\text{jet}}|$  are shown in Figure 15. The top row shows the predictions of a model in which all jets have identical upstream Lorentz factors of 5, while the middle and bottom rows show values of 15 and 25, respectively. The most prominent feature of these dis-

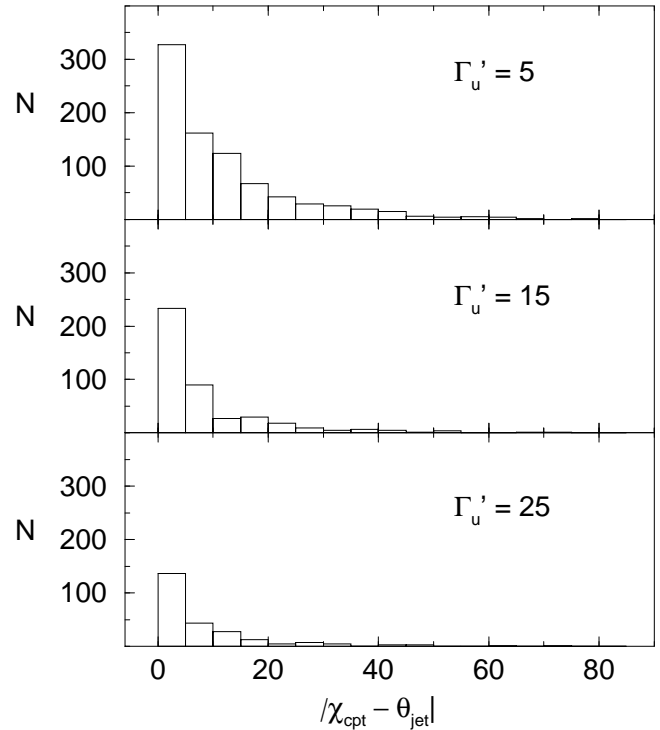


FIG. 15.—Simulated distributions of the misalignment angle  $|\chi - \theta|$  between the electric vector position angle of strongly shocked components and the local jet direction for a population of moving oblique shocks. The top row uses a population of jets with upstream Lorentz factors of 5, while the middle and bottom rows use  $\Gamma'_u = 15$  and 25, respectively.

tributions is that they are highly peaked at low misalignment values. Although the probability distribution for  $\eta$  does favor more transverse shocks, the main reason for the peaks in Figure 15 is the Lorentz transformation of the obliqueness angle from the shock frame to the rest frame of the upstream flow:  $\tan \eta_{\text{up}} = \Gamma_{\text{up}} \tan \eta$ . If the upstream flow is highly relativistic (as is thought to be the case for blazar jets), the obliqueness angle  $\eta$  will be nearly perpendicular to the jet axis in the upstream frame. This configuration then leads to an EVPA that is aligned with the jet. As this is the dominant effect, the distribution of shock velocity (in the observer frame) should have very little effect on the distributions in Figure 15. We have confirmed this using additional simulations (not shown).

Another consequence of the Lorentz transformation for  $\eta$  in high- $\Gamma$  jets is that in a flux-limited sample that favors small viewing angles, more shocks will be effectively seen face on. As a result, these are likely to have fractional polarizations of less than 1%, and will be excluded from our simulated populations. For this reason, the bottom two panels of Figure 15 contain fewer shocks than the top panel.

## 6. ALTERNATIVES TO OBLIQUE SHOCKS

Our simulations show that the predicted EVPA misalignment distribution of a single population of oblique shocks is highly peaked near zero as a result of relativistic effects. However, the distribution of component EVPA misalignments in the inner jets of blazars (Fig. 14) is relatively flat.

As an alternative to the oblique shock model, we consider a possible (yet less physical) scenario involving regions of

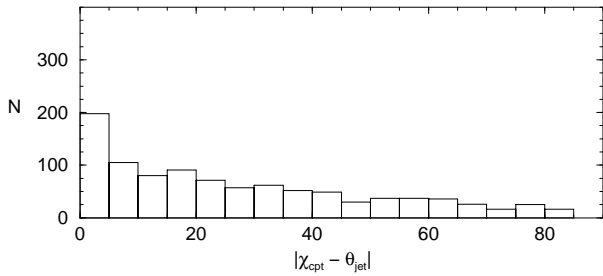


FIG. 16.—Simulated distribution of electric vector misalignment angle for a population of enhanced emitting regions moving at the jet bulk flow speed of  $\beta = 0.9798$  ( $\Gamma = 5$ ). Each region has a fixed electric field direction, oriented at an arbitrary angle to the jet axis. The form of the above distribution is independent of  $\beta$ .

enhanced number density and/or magnetic field that propagate down the jet at the bulk flow speed with a fixed magnetic field configuration. Such disturbances are likely to evolve into shocks after this period of quasi-ballistic motion. As in the shock model, we require the magnetic field of these regions to be enhanced along a particular plane oriented at angles  $\eta$  and  $\phi$  in the jet frame. Since the emitting gas is moving parallel to the jet axis in this case, no transformation of the obliqueness angle  $\eta$  is required as before, which has a profound effect on the predicted EVPA misalignment distributions.

In Figure 16 we show the predicted distribution of misalignment angles for a population of these regions using the same parameters as in the previous models, with  $\Gamma = 5$ , and  $0^\circ \leq \eta \leq 90^\circ$ . The form of the distribution remains the same for larger Lorentz factors. When the mean Lorentz factor of a jet population is increased, a flux-limited sample becomes more biased toward jets with end-on orientations, as measured in the observer frame (eq. [3]). However, in the *comoving* frame, the viewing angle distribution is independent of  $\Gamma$ .

This particular model predicts a much smaller bias toward aligned EVPAs than the shock models in Figure 15, since there is no Lorentz transformation of the angle  $\eta$ . The model still predicts a slight peak at zero, owing to the probability distribution we have used for  $\eta$ . A better fit to the data might be obtained by using an  $\eta$  distribution that is biased toward smaller values, for example. It is unclear, however, what physical process or processes in a jet might give rise to such a distribution. More data on the polarized regions of blazar jets are needed to constrain these models further.

Our hypotheses can be tested by studying the evolution of both the EVPAs and the fractional polarizations of oblique components as they propagate down the inner jets of blazars. Such studies could determine whether more oblique shocks in fact have slower velocities (as predicted by the shock model), and how the EVPA changes as a function of distance along the jet. In a multiepoch study of 3C 345 at centimeter wavelengths, Brown et al. (1994) found that the EVPA of one component remained parallel to the jet as it traveled outward on a curved trajectory, while another component maintained a consistently oblique EVPA. Similarly, the superluminal component C5 in our image of OJ 287 appears to maintain the same oblique EVPA in observations spaced one year apart (see § 3.2.2). These somewhat contradictory findings indicate that the magnetic field orientations of VLBI components may be

considerably more complex than the predictions of the simple transverse shock model.

## 7. CONCLUSIONS

An important result of this study is that for all of the high optical polarization quasars (HPQs) in our sample, the inferred magnetic field orientation of the core was found to be perpendicular to the jet. This is in direct contrast to observations at lower frequencies, where quasars have predominantly aligned magnetic fields, while in BL Lacs they are perpendicular to the jet (Gabuzda et al. 1994; Cawthorne et al. 1993). The latter authors have suggested that in some quasars there may be sufficiently strong shocks in the inner jet that would dominate an underlying longitudinal field and change the magnetic field orientation to perpendicular. This interpretation would therefore suggest that all of the HPQs in our sample have unresolved shocks near the base of the jet. It is unclear from our data whether this also holds true for BL Lacs. Multiepoch high-resolution data on larger samples are required to determine whether, for example, some HPQs and BL Lacs have highly polarized standing shocks near the core that would dominate the polarization properties and lead to stable EVPAs such as those seen in 0829+046, 1055+018, and 1334–127. These shocks would partially cancel out longitudinally polarized emission from the inner jet, thereby lowering the fractional polarization of the core. Such structures might also be responsible for determining whether an object has high or low optical polarization, as hinted by the parallel  $B$  field seen in the core of the LPQ 1611+343.

Our high-frequency polarization images have also demonstrated that components with oblique EVPAs (with respect to the jet axis) are common in the parsec-scale jets of blazars. We have shown that the observed EVPA distribution is inconsistent with a population of moving, oblique shocks. The latter model predicts an overabundance of components with aligned EVPAs, as a result of relativistic effects associated with the jet flow. The data are more consistent with a nonshock model, in which the polarized jet components are merely enhanced regions whose magnetic field orientations are determined by some mechanism other than shocks.

Finally, we have shown that with the advent of the VLBA and improved routines in AIPS, it is now possible to obtain high-frequency polarization-sensitive VLBI observations of moderately large samples of bright AGNs with a reasonable amount of effort and observing time. As more such observational programs are carried out, much greater insight will be gained into the magnetofluid dynamics in the inner jets of quasars and BL Lac objects.

The authors wish to thank the referee, John Wardle, for a careful reading of the original manuscript and valuable discussions that greatly improved this paper. We also thank David Clarke for helpful discussions regarding oblique shocks. This work was supported in part by NASA grants NAG 5-4245 and NAG 5-3829, and has made use of data from the NASA/IPAC Extragalactic Database (NED), operated by the Jet Propulsion Laboratory, California Institute of Technology, under contract to the National Aeronautics and Space Administration, and from the University of Michigan Radio Astronomy Observatory, which is supported by the National Science Foundation and by funds from the University of Michigan.

## REFERENCES

- Alberdi, A., et al. 1997, *A&A*, 327, 513
- Aller, H. D., Aller, M. F., Latimer, G. E., & Hodge, P. E. 1985, *ApJS*, 59, 513
- Altschuler, D. R., Broderick, J. J., Dennison, B., Mitchell, K. J., Odell, S. L., Condon, J. J., & Payne, H. E. 1984, *AJ*, 89, 1784
- Antonucci, R. R. J., & Ulvestad, J. S. 1985, *ApJ*, 294, 158
- Attridge, J. M., Roberts, D. H., & Wardle, J. F. C. 1998, in *IAU Colloq. 164, Radio Emission from Galactic and Extragalactic Compact Sources* (Dordrecht: Reidel), in press
- Bajkova, A. T., Pyatunina, T. B., & Finkelstein, A. M. 1996, *Commun. Inst. Appl. Astron.*, No. 87
- Bicknell, G. V., & Begelman, M. C. 1996, *ApJ*, 467, 597
- Blandford, R. D., & Königl, A. 1979, *ApJ*, 232, 34
- Bondi, M., et al. 1996, *A&A*, 308, 415
- Brinkmann, W., Siebert, J., Reich, W., Fuerst, E., Reich, P., Voges, W., Truemper, J., & Wielebinski, R. 1995, *A&AS*, 109, 147
- Brotten, N. W., MacLeod, J. M., & Vallee, J. P. 1988, *Ap&SS*, 141, 303
- Brown, L. F., Roberts, D. H., & Wardle, J. F. C. 1994, *ApJ*, 437, 108
- Carini, M. T., Miller, H. R., Noble, J. C., & Sadun, A. C. 1991, *AJ*, 101, 1196
- Carrara, E. A., Abraham, Z., Unwin, S. C., & Zensus, J. A. 1993, *A&A*, 279, 83
- Carvalho, J. C. 1985, *A&A*, 150, 129
- Cawthorne, T. V., & Cobb, W. K. 1990, *ApJ*, 350, 536 (CC90)
- Cawthorne, T. V., & Gabuzda, D. C. 1996, *MNRAS*, 278, 861
- Cawthorne, T. V., Wardle, J. F. C., Roberts, D. H., & Gabuzda, D. C. 1993, *ApJ*, 416, 519
- Charlot, P. 1990, *A&A*, 229, 51
- Comastri, A., Fossati, G., Ghisellini, G., & Molendi, S. 1997, *ApJ*, 480, 534
- Conway, J. E., & Wrobel, J. M. 1995, *ApJ*, 439, 98
- Dallacasa, D., Fanti, C., Fanti, R., Schilizzi, R. T., & Spencer, R. E. 1995, *A&A*, 295, 27
- Fey, A. L., Clegg, A. W., & Fomalont, E. B. 1996, *ApJS*, 105, 299
- Fichtel, C. E., et al. 1994, *ApJS*, 94, 55
- Gabuzda, D. C., & Cawthorne, T. V. 1996, *MNRAS*, 283, 759
- Gabuzda, D. C., Mullan, C. M., Cawthorne, T. V., Wardle, J. F. C., & Roberts, D. H. 1994, *ApJ*, 435, 140
- Gear, W. K., et al. 1994, *MNRAS*, 267, 167
- Gómez, J., Marscher, A. P., Alberdi, A., Martí, J. M., & Ibáñez, J. M. 1998, *ApJ*, 499, 221
- Holmes, P. A., Brand, P. W. J. L., Impey, C. D., & Williams, P. M. 1984, *MNRAS*, 210, 961
- Homan, D. C., Wardle, J. F. C., Ojha, R., & Roberts, D. H. 1998, in *IAU Colloq. 164, Radio Emission from Galactic and Extragalactic Compact Sources* (Dordrecht: Reidel), in press
- Hughes, P. A., Aller, H. D., & Aller, M. F. 1985, *ApJ*, 298, 301
- Impey, C. D., & Neugebauer, G. 1988, *AJ*, 95, 307
- Impey, C. D., & Tapia, S. 1990, *ApJ*, 354, 124
- Junor, W., Mantovani, F., Peck, A., Saikia, D., & Salter, C. 1996, in *IAU Symp 175, Extragalactic Radio Sources*, ed. R. Ekers, C. Fanti, & L. Padrielli (Dordrecht: Kluwer), 79
- Kellermann, K. I., Vermeulen, R. C., Zensus, J. A., & Cohen, M. C., 1998, *AJ*, 115, 1295
- Kemball, A. J., Diamond, P. J., & Pauliny-Toth, I. I. K. 1996, *ApJ*, 464, L55
- Königl, A. 1980, *Phys. Fluids*, 23, 1083
- Krichbaum, T. P., Witzel, A., Standke, K. J., Graham, D. A., Schalinski, C. J., & Zensus, J. A. 1994, in *Compact Extragalactic Radio Sources*, ed. J. A. Zensus & K. I. Kellermann (Charlottesville: NRAO), 39
- Kühr, H., & Schmidt, G. D. 1990, *AJ*, 99, 1
- Laing, R. A. 1980, *MNRAS*, 193, 439
- Leppänen, K. J. 1995, Ph.D. thesis, Helsinki Univ. of Technology
- Leppänen, K. J., Zensus, J. A., & Diamond, P. J. 1995, *AJ*, 110, 2479
- Lind, K. R., & Blandford, R. D. 1985, *ApJ*, 295, 358
- Lister, M. L. 1998, Ph.D. thesis, Boston Univ.
- Lobanov, A. I. 1998, *A&A*, 330, 79
- Marscher, A. P., & Gear, W. K. 1985, *ApJ*, 298, 114
- Marscher, A. P., & Marchenko, S. V. 1997, in *Multifrequency Monitoring of Blazars*, ed. G. Tosti & L. Takalo (Perugia Univ. Obs. Publ. No. 3) 68
- Marscher, A. P., Marchenko, S. V., Wehrle, A. E., & Xu, W. 1998, in *IAU Colloq. 164, Radio Emission from Galactic and Extragalactic Compact Sources* (Dordrecht: Reidel), in press
- McLaughlin, M. A., Mattox, J. R., Cordes, J. M., & Thompson, D. J. 1996, *ApJ*, 473, 763
- Morganti, R., Killeen, N. E. B., & Tadhunter, C. N. 1993, *MNRAS*, 263, 1023
- Murphy, D. W., Browne, I. W. A., & Perley, R. A. 1993, *MNRAS*, 264, 298
- Mutel, R. L., Su, B., Bucciferro, R. R., & Phillips, R. B. 1990, *ApJ*, 352, 81
- Nartallo, R., Gear, W. K., Murray, A. G., Robson, E. I., & Hough, J. H. 1998, *MNRAS*, in press
- National Radio Astronomy Observatory. 1990, *The AIPS Cookbook* (Charlottesville: NRAO)
- O'Dea, C. P., Baum, S. A., & Stanghellini, C. 1991, *ApJ*, 380, 66
- O'Dea, C. P., Baum, S. A., Stanghellini, C., Morris, G. B., Patnaik, A. R., & Gopal-Krishna. 1990, *A&AS*, 84, 549
- Ojha, R. 1997, Ph.D. thesis, Brandeis Univ.
- Padrielli, L., Mantovani, F., Eastman, W., Spangler, S., & Gregorini, L. 1991, *A&A*, 249, 351
- Padrielli, L., et al. 1986, *A&A*, 165, 53
- Perley, R. A. 1982, *AJ*, 87, 859
- Pica, A., Smith, A. G., Webb, J. R., Leacock, R. J., Clements, S., & Gombola, P. P. 1988, *AJ*, 96, 1215
- Piner, B. G., & Kingham, K. A. 1997, *ApJ*, 479, 684 (PK97)
- Reuter, H.-P., et al. 1997, *A&AS*, 122, 271
- Romney, J., et al. 1984, *A&A*, 135, 289
- Sambruna, R. M., et al. 1997, *ApJ*, 474, 639
- Shepherd, M. C., Pearson, T. J., & Taylor, G. B. 1994, *BAAS*, 26, 987
- Sitko, M. L., Schmidt, G. D., & Stein, W. A. 1985, *ApJS*, 59, 323
- Smith, P. S., Balonek, T. J., Elston, R., & Heckert, P. A. 1987, *ApJS*, 64, 459
- Spangler, S. R., Mutel, R. L., & Benson, J. M. 1983, *ApJ*, 271, 44
- Sreekumar, P., et al. 1996, *ApJ*, 464, 628
- Stanghellini, C., Baum, S. A., O'Dea, C. P., & Morris, G. B. 1990, *A&A*, 233, 379
- Steffen, W., Zensus, J. A., Krichbaum, T. P., Witzel, A., & Qian, S. J. 1995, *A&A*, 302, 335
- Stevens, J. A., Litchfield, S. J., Robson, E. I., Hughes, D. H., Gear, W. K., Teräsraanta, H., Valtaoja, E., & Tornikoski, M. 1994, *ApJ*, 437, 91
- Stickel, M., Kühr, R., & Fried, J. W. 1993, *A&AS*, 97, 483
- Stickel, M., Meisenheimer, K., & Kühr, H. 1994, *A&AS*, 105, 211
- Teräsraanta, H., & Valtaoja, E. 1994, *A&A*, 283, 51
- Tornikoski, M., et al. 1996, *A&AS*, 116, 157
- Tornikoski, M., Valtaoja, E., Terasranta, H., Lainela, M., Bramwell, M., & Botti, L. C. L. 1993, *AJ*, 105, 1680
- Tornikoski, M., Valtaoja, E., Terasranta, H., Smith, A. G., Nair, A. D., Clements, S. D., & Leacock, R. J. 1994, *A&A*, 289, 673
- Vermeulen, R. C., & Cohen, M. H. 1994, *ApJ*, 430, 467
- Vicente, L., Charlot, P., & Sol, H. 1996, *A&A*, 312, 727
- Wardle, J. F. C., & Kronberg, P. 1974, *ApJ*, 194, 249
- Weekes, T. C., et al. 1996, *A&AS*, 120, 603
- Wehrle, A. E., et al. 1998, *ApJ*, submitted
- Wills, D., Wills, B. J., Breger, M., & Hsu, J.-C. 1980, *AJ*, 85, 1555